Adaptive Band-Partitioning for

Interference Cancellation in Communication Systems

by

Michael A. Leabman

Submitted to the Department of Electrical Engineering and Computer Science
in Partial Fulfillment of the Requirements for the Degrees of
Bachelor of Science in Electrical Science and Engineering
and
Master of Engineering in Electrical Engineering and Computer Science
at the
MASSACHUSETTS INSTITUTE OF TECHNOLOGY
February, 1997

Author ______________________________

Department of Electrical Engineering and Computer Science
February, 1997

Certified by ______________________________

David H. Staelin
Professor of Electrical Engineering

Accepted by ______________________________

A.C. Smith
Chairman, Department Committee on Graduate Thesis

Adaptive Band-Partitioning for Interference Cancellation in Communication Systems

by

Michael A. Leabman

Submitted to the Department of Electrical Engineering and Computer Science

February, 1997

in partial fulfillment of the requirements for the degrees of

Bachelor of Science in Electrical Science and Engineering and

Master of Engineering in Electrical Engineering and Computer Science

Abstract

Adaptive signal processing using an array of antenna elements has long been a solution to the problem of combating interference in communication systems. While the classical method of applying a complex weight to each array element has proven very effective for cancellation of interference signals, it has its limitations. The performance is degraded in the presence of interference signals of reasonable bandwidth. In addition, the angle of arrival of the unwanted signals leads to further loss of interference rejection. With the advent of inexpensive high speed computers, new adaptive systems never before capable of implementation are being explored. One such approach, named adaptive band-partitioning, attempts to alleviate the problems of the classical approach by applying frequency-dependent complex weights. In addition to its insensitivity to interference bandwidth and angle of arrival, this approach is shown to have the capability of canceling a far greater number of interference signals than traditional methods. Whereas fixed-weight methods performed on a N-element array are limited to the ability of canceling N-1 interference signals, provided they have bandwidths much less than the signal bandwidth, adaptive band-partitioning can be shown to cancel up to (N-1)L/2 signals where the interference signals are narrowband and L is the number of bins used in dividing the frequency spectra. It can be demonstrated that adaptive band-partitioning is a viable solution to the problem of interference cancellation.

Thesis Advisor: Dr. David H. Staelin

Title: Professor of Electrical Engineering, Massachusetts Institute of Technology

Acknowledgments

There are several people who have made this thesis possible. I would like to begin by thanking my advisor Professor David Staelin, whose comments were pertinent, encouraging, and quite prompt. Most importantly, I would like to thank my parents. Their optimism and confidence in me has gotten me through the tough times at MIT. Without their constant love and support, I would never had made it this far. Mom and Dad, this one's for you. The final person I want to thank is my the love of my life, Maya. Thank you for taking the time to listen to my numerous attempts at explaining my thesis. It really helped me focus my thoughts and become much more productive. I Love You.

Table of Contents

List of Figures

Chapter 1

1. Introduction

Adaptive signal processing using an array of elements has long been a solution to the problem of combating interference signals in communication systems. However, in the last few years with the introduction of compact, inexpensive digital computers, it is now feasible to implement more complicated results from detection and estimation theory. These results have led to the development of adaptive array systems that can adjust and respond to a changing signal environment. As a consequence, systems with much greater flexibility, reliability, and improved reception than previous systems can be realized.

1.1 Motivation for Adaptive Arrays

In recent years, adaptive arrays have become a significant area of study for their effectiveness in reducing interference signals present in radar, sonar, and communication systems. Where common filter techniques using one element have proven to be effective when frequencies of interest differ from the frequencies of interference signals, adaptive array algorithms have become commonplace when the spectrum of interference signals and the desired signal overlap. Since an adaptive array has the ability to automatically sense and separate signals and interference noise from different directions without prior knowledge of the environment, it has become of widespread interest. Furthermore, adaptive arrays can be used in conjunction with other interference reduction techniques, thus achieving a reduction greater than can be accomplished by using just one method.

In conventional communication systems, a direct-sequence spread-spectrum system is often utilized, modulating the communication signal with a pseudonoise(PN) signal and later despreading it with the original known PN sequence. While this conventional method can reduce interference, it is limited by the length of the PN sequence. The longer the PN code, the greater the ability to separate the signal from the interference noise. Since longer PN sequences also result in longer transmission delays, the length of the PN code and thus the ability to cancel noise is often limited. As this is frequently the case, another method, such as that of the adaptive array system, is often implemented in conjunction with the spread-spectrum approach when further interference attenuation and greater channel capacity is desired.

1.2 Adaptive Band-Partitioning Approach

While classical adaptive array methods have proven to be very effective for cancellation of interference signals, they are still plagued by several severe limitations. The ability of such a system to cancel interference signals is strongly influenced by the arrival angle and bandwidth of the interference signals. To alleviate these problems, an adaptive system, one which applies multiple frequency-dependent weights to each array element rather than just one weight on each element, is proposed which should provide numerous benefits over the older more classical approaches. This approach, known as adaptive band-partitioning, divides the frequency spectrum into multiple narrow frequency bins and then performs spatial cancellation on each bin. The primary advantage of this approach is the ability to cancel interference signals of appreciable bandwidths. Furthermore, the system also has the ability to cancel a greater number of narrowband interference signals. While the classical approach is capable of attenuating N-1 narrowband interference signals, N being the number of antenna elements in the array, the new proposed system has the ability of attenuating N-1 narrowband interference signals in each frequency bin.

1.3 Overview

The overall goal of this thesis is to determine the ability of adaptive band-partitioning to cancel interference signals. To do so, we first need to establish the basic characteristics and capabilities of an array. Chapter 2 begins by investigating the properties of an array. Here, we see how the performance of an adaptive array as a spatial filter is characterized by two important aspects, the spacing and size of the array. Then, we introduce the classical array approach to interference cancellation by introducing complex weights to each element of the array. The classical approach's ability to reject and cancel unwanted interference signals are discussed in detail.

While Chapter 2 illustrates the ability of complex weights to aid in the cancellation of interference signals, Chapter 3 investigates the methods and algorithms used in determining the correct set of weights. The two most widely used methods of deriving the optimal steady-state weights, the mean-square-error criterion (MSE) and the maximum likelihood criterion (ML) are derived. Since in most applications the signal environment changes over time, we are then left with the problem of developing an algorithm for the weights that converges as quickly as possible to the optimal steady-state weights. For this reason, two adaptive algorithms, the least-mean-square (LMS) and direct matrix inversion (DMI), are then studied.

Chapter 4 describes the derivation of, and implications of implementing adaptive band-partitioning. Finally, simulations are performed and analyzed to assess the true ability of adaptive band-partitioning to cancel interference signals. Specific cases, involving narrowband and wideband interference signals, are examined to fully characterize the functionality and practicality of such a system.

Chapter 2

2. Adaptive Array Concept and Performance

The performance of an adaptive array as a spatial filter is characterized by two important aspects. The arrangement and spacing of the array elements constrain the basic operation of the array while the design of the complex weighting of the data from each array element determines the ability of the adaptive array to reject unwanted signals.

2.1 Element Spacing Constraints

First, we must investigate the variables used in representation of spatial coordinates. Most array literature specifies spatial dependence in terms of the more intuitive 'angle'; however, it is more powerful to introduce the wavenumber variable $\vec{k}$ [1] where, $|\vec{k}| = \omega / c$, ω being the radian frequency ($2\pi f$) , and c being the propagation speed in free space. Thus $|\vec{k}| = \omega / c = 2\pi f/c = 2\pi/\lambda$,[2] and has dimensions of 1/length. While the standard angular representation does describe the response over the region for all real signals, the full wavenumber space, or "virtual" space, is more useful in analyzing the consequences of spatial aliasing.

Let us now consider an array of N sensors sampling an area of space where the element locations are governed by $[\vec{z}_i, i = 1,..,N]$. From this we have a time series $x(t, \vec{z}_i)$ as illustrated in Figure 2.1. Then, the output from each sensor is input to a linear, time invariant filter having the impulse response $w_i(\tau)$. Finally, the outputs of the filters are summed to produce the output of the array y(t),

$$y(t) = \sum_{i=1}^{N} \int_{-\infty}^{\infty} w_i(t - \tau) x(\tau, \vec{z}_i) d\tau \, . \tag{2.1}$$

---

[1] → represents a spatial vector in terms of (x,y,z).

[2] Where the wavelength $\lambda = f/c$ and $c = 3*10^8$m/s for radio waves.

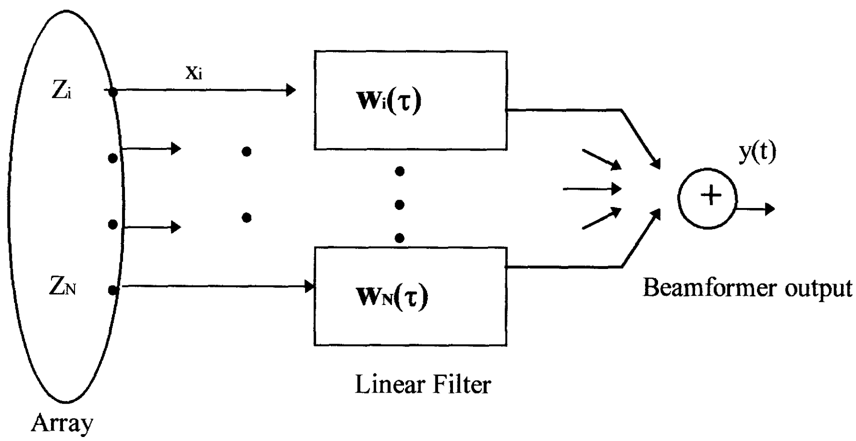

Figure 2.1 Beamforming Model.

Using the Fourier representation for a space-time signal, a plane wave $x(t, \vec{z}_i)$ of a single frequency can be represented by a complex exponential in terms of a radian frequency ω, and vector wavenumber $\vec{k}$:

$$x(t, \vec{z}_i) = e^{j(\omega t - \vec{k} \cdot \vec{z}_i)} \text{ .}^{3} \tag{2.2}$$

The array response to a plane wave is as follows:

$$y(t) = \sum_{i=1}^{N} \int_{-\infty}^{\infty} w_i(t-\tau) x(\tau, z_i) d\tau$$

$$= \sum_{i=1}^{N} \int_{-\infty}^{\infty} w_i(t-\tau) e^{j(\omega\tau - \vec{k}\cdot\vec{z}_i)} d\tau$$

---

[3] T represents transpose, + complex conjugate transpose

$$= \sum_{i=1}^{N} \int_{-\infty}^{\infty} w_i(t')e^{-j\omega t'} e^{-j\vec{k}\cdot\vec{z}_i} e^{j\omega t} dt' \quad \text{where } \tau = t - t'$$

$$= \sum_{i=1}^{N} w_i(\omega) e^{j(\omega t - \vec{k}\cdot\vec{z}_i)} \qquad \textbf{(2.3)}$$

Letting

$$\mathbf{W}(\omega) = \begin{bmatrix} w_1(\omega) \\ \vdots \\ \vdots \\ w_N(\omega) \end{bmatrix} \quad \text{and} \quad \mathbf{E}(k) = \begin{bmatrix} e^{-j\vec{k}\cdot\vec{z}_1} \\ e^{-j\vec{k}\cdot\vec{z}_2} \\ \vdots \\ e^{-j\vec{k}\cdot\vec{z}_N} \end{bmatrix} \qquad \textbf{(2.4)}$$

(2.3) becomes $$y(t) = \mathbf{W}^+(\omega)\mathbf{E}(k)e^{j\omega t} \qquad \textbf{(2.5)}$$

where $W(\omega,\vec{k}) = \mathbf{W}^+(\omega)\mathbf{E}(k)$ is the frequency wavenumber response.[4] The frequency wavenumber response evaluated versus direction $\vec{k}$, is known as the beampattern,

$$B(a(\theta,\phi)) = W(\omega,\vec{k})\Big|_{\vec{k}=\frac{2\pi}{\lambda}a(\theta,\phi)}, \qquad \textbf{(2.6)}$$

where $\mathbf{a}(\theta,\phi)$ is the unit vector in spherical coordinates.

The most widely used array, due to its simplicity and well known characteristics, is a linear uniformly weighted array with N elements and an inter-element spacing of Δz.

---

[4] Throughout this thesis, a variable will be bold if it represents a vector.

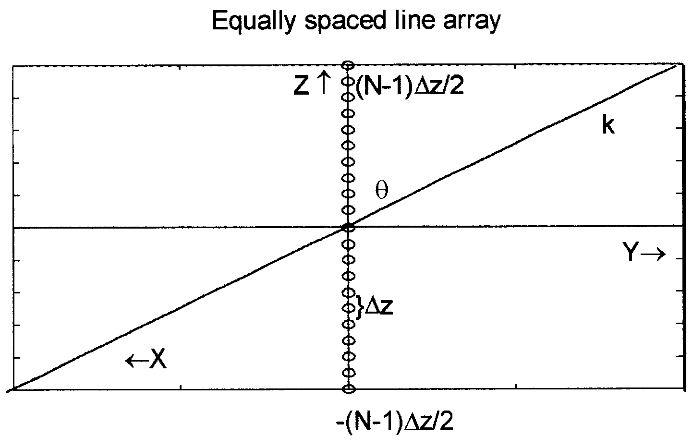

Figure 2.2 Uniform Line Array along z-axis

If we use a frequency independent uniform weighting of 1/N, we arrive at a frequency wavenumber response[5]

$$W(\omega, k) = \frac{1}{N} \sum_{n=-\frac{N-1}{2}}^{\frac{N-1}{2}} e^{-j\vec{k}\cdot\hat{a}_z n \Delta z} \text{, where } \vec{k}\cdot\hat{a}_z = k_z$$

$$= \frac{\sin c(k_z \frac{L}{2})}{\sin c(k_z \frac{\Delta z}{2})}. \qquad \textbf{(2.7)}$$

Evaluating (2.7) for $k_z = |k|\sin(\theta) = \frac{2\pi}{\lambda}\sin(\theta)$, where θ is defined with respect to the angle to the z axis, we arrive at a beampattern of

---

[5] sinc(x)=sin(x)/x,

$$B(\omega,\theta)=\frac{\operatorname{sinc}\left(2\pi\sin(\theta)\frac{L}{2\lambda}\right)}{\operatorname{sinc}\left(2\pi\sin(\theta)\frac{\Delta z}{2\lambda}\right)},\text{ where L=N}\Delta\text{z.} \quad \textbf{(2.8)}$$

Due to the spatial sampling of our discrete array, we observe grating lobes in Figure 2.3 at integer multiples of k=2π/Δz. If the element spacing Δz is greater than λ, the grating lobes would appear within the region of propagating signals, or rather 'real space'. In order to

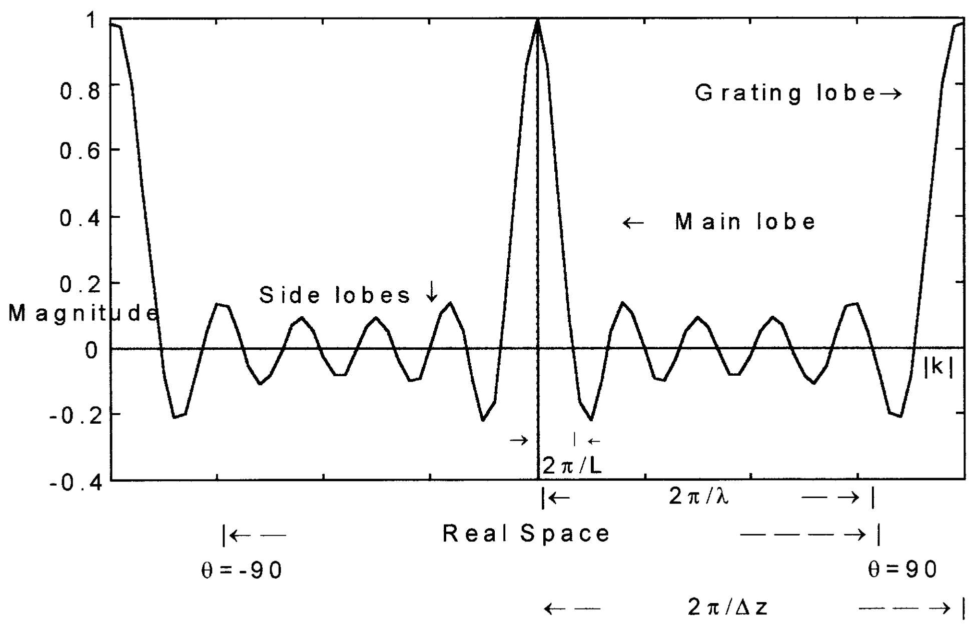

Figure 2.3 Beampattern response for linear array and uniform weighting.

avoid such aliasing, we require Δz<λ/2, known as the spatial Nyquist criterion. We must keep in mind, however, that the resolution of the main lobe is 2π/L = 2π/NΔz and thus the smaller the spacing Δz, the worse the resolution. In practice, the spacing is chosen as big as possible while still avoiding aliasing, hence we choose Δz=λ/2.

We have just seen how element spacing determines the array's resolution and grating lobe effects. Now, let us examine how the number of elements affects array performance. Having constrained Δz=λ/2, our array's resolution, 2π/NΔz, is now completely determined by the number of elements. In addition, as we increase N, the number of nulls in real space increases. To illustrate this dependence, let us examine some beampattern responses for linear spaced arrays with uniform weighting and a spacing $\Delta z=\lambda/2$. In Figure 2.4, the nulls occur at $\theta=\pm 90°$ due to the fact that the signal wavefront at that direction of arrival travels exactly $\lambda/2$[6] between the two array elements.

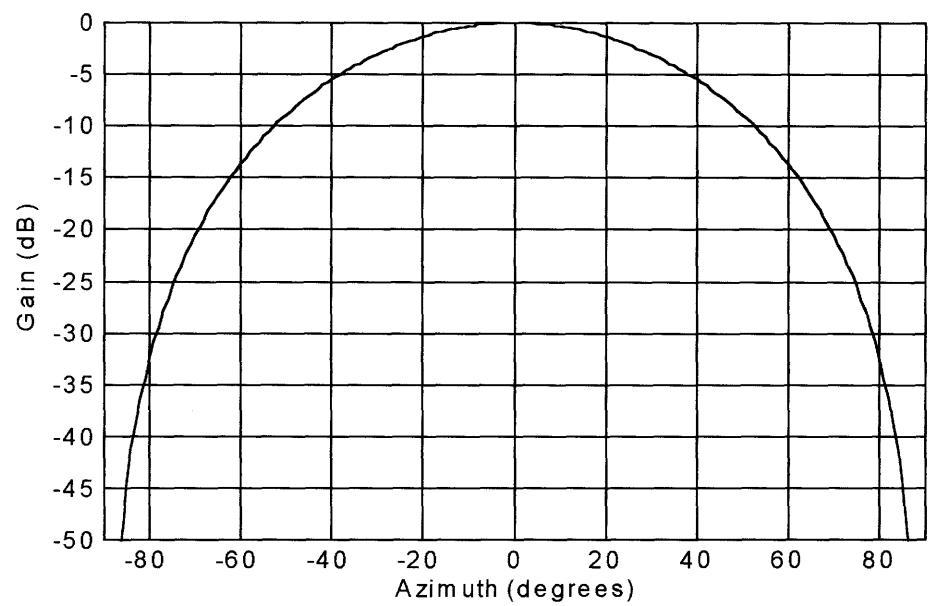

Figure 2.4 Array beampattern for two-element array.

The signals at the two elements differ by a phase shift of 180°, and thus the array sum results in an exact cancellation of the signal. As we increase the number of array elements, Figure 2.5, the placement of the nulls change according to the beampattern equation, with nulls at

$$\theta_m = m \cdot \sin^{-1}(2/N)\ , \quad \text{m} = \pm 1, 2, 3, \ldots \text{N}/2 \text{ and N odd.} \qquad \textbf{(2.9)}$$

Notice that the level of the first sidelobes are -13.5dB down from the mainlobe. This is due to our uniform weighting. If we were, however, to use an non-uniform window, or

[6] Up till now, we have assumed that f in $\lambda=c/f$, is the single center frequency.

taper, such as a Hamming or Kaiser-Besssel window, we could lower the first sidelobes to -50dB or -80dB, respectively.

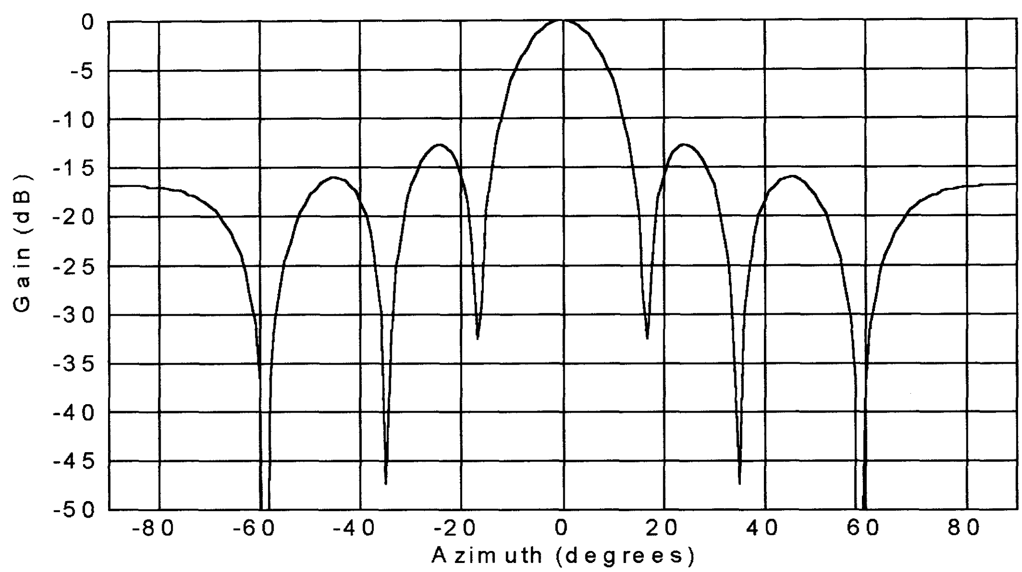

Figure 2.5 Beam pattern for seven-element array.

For interference signals not in the mainlobe, we would have excellent rejection or cancellation. Unfortunately there is always a tradeoff, and by decreasing the sidelobes we have drastically increased the width of our mainlobe. See *Oppenheim and Schafer* for windowing effects.

While the mainlobe resolution and number of nulls increase with the number of elements N, the widths or sharpness of the nulls actually decrease with N, and thus the ability of the array to place a broad null on aggregate interference sources degrades. However, as we will soon discover in Section 2.2, by choosing appropriate weights the array beam pattern nulls can be placed arbitrarily in whatever single direction one wishes to cancel interference signals. In addition, by inserting a time delay of $n\lambda/2 \cdot \sin(\theta steer)$, or an equivalent phase shift, in each nth element, we can "steer" the array beam pattern so that the entire pattern is shifted over by θ. The resulting steered beampattern is

$$B(\omega,\theta) = \frac{\sin c\left(2\pi\{\sin(\theta) - \sin(\theta_{steer})\}\frac{L}{2\lambda}\right)}{\sin c\left(2\pi\{\sin(\theta) - \sin(\theta_{steer})\}\frac{\Delta z}{2\lambda}\right)}. \qquad \textbf{(2.10)}$$

For a θsteer=15°, we have the resulting plot:

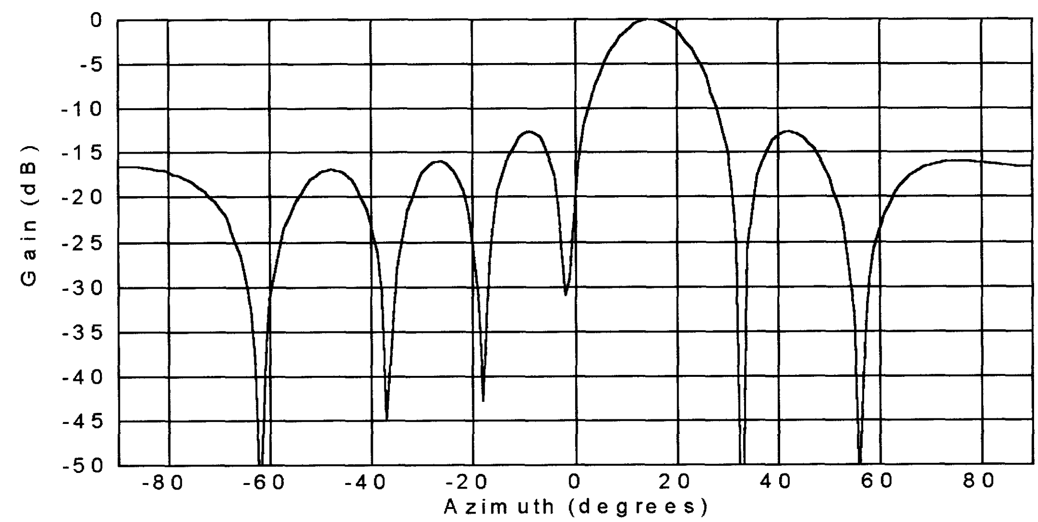

Figure 2.6 Beampattern for array steered to 15°.

While the operation of delaying or advancing the signal by adjusting the weights w(τ) can effectively steer the beampattern, it can also produce a destructive combination, or null, at a particular angle θ.

2.2 Classical Two-Element Interference Cancellation

Consider a two-element linearly spaced array separated by a spacing of Δz, shown below in Figure 2.7. An interference signal n(t) originating from a direction θ arrives at the second element τ seconds later that the first element, where τ=(Δz/c)sinθ and c=propagation speed.

If we sum the signals from the two elements, ignoring the weights for now, the resulting output y(t)= n(t) + n(t-τ). To truly cancel n(t), all we would really need to do is delay the signal received at element one by τ and subtract this from the signal received at element two. While this would result in perfect cancellation of all frequencies at an angle θ, in practice the angle of arrival is not known, and thus there is no straight forward method for determining the time delay needed.

However, as we will see in Chapter 3, by introducing a complex weight[7] on each array element, we can devise a method for determining the directions of signal wavefronts.

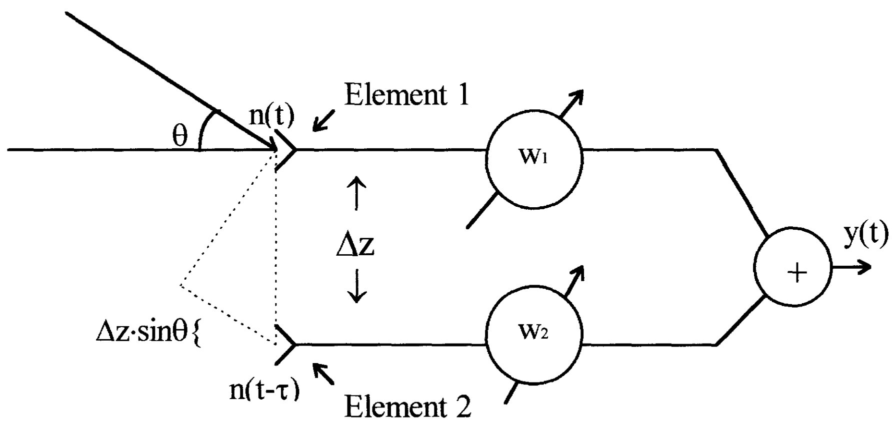

Figure 2.7 Two-Element Linear Array.

2.3 Nulling Limitations

Assuming for now that we know the angle of arrival for a single interference signal n(t), let us again refer to Figure 2.7. If we form the output y(t), but now add the effect of the complex weights,

$$y(t) = w_1 n(t) + w_2 n(t - \tau). \tag{2.11}$$

Taking the Fourier transform, the frequency domain representation is:

---

[7] W is a complex number, $W = w_{real} + jw_{imaginary}$.

$$Y(\omega,t) = N(\omega,t)[w_1 + w_2 e^{-j\omega\tau}]. \quad \textbf{(2.12)}$$

If the interference is a stationary signal, where the frequency spectra N(ω,t) varies slowly over time relative to ω, and narrowband with a center frequency of f_o, N(ω,t) would be zero everywhere except where ω equals ω_o. To perfectly cancel the signal, all we need to do is choose

$$w_1 = -w_2 e^{-j\omega_o\tau}. \quad \textbf{(2.13)}$$

With these weights, Y(ω,t)=0.

2.3.1 Bandwidth Degradation

In most situations though, the interference signal one encounters is not a narrowband signal, but a signal with some bandwidth. Using the above weights now results in less than perfect cancellation. For a perfectly stationary environment N(ω,t)=N(ω) and the weights result in a transfer function

$$H(\omega) = \frac{Y(\omega)}{N(\omega)} = w_1[1 - e^{-j(\omega-\omega_o)\tau}]. \quad \textbf{(2.14)}$$

If we let $|w_1|^2 = 1$, the output power $|H(\omega)|^2$ becomes,

$$|H(\omega)|^2 = \{2 - 2\cos[\tau(\omega - \omega_o)]\}. \quad \textbf{(2.15)}$$

The plot of the output interference spectrum (for $\Delta z=\lambda o/2$ and $\theta=90°$) is seen in Figure 2.8. Ignoring the internal thermal noise associated with an array element, the output spectrum is perfectly zero, as we expected, at the center frequency of 100 MHz , but increases rapidly as we move away from the center frequency of the interference signal.

For an interference signal with a bandwidth, the frequencies away from the center frequency will only be attenuated and not completely canceled. As illustrated in Figure 2.8, a signal with a bandwidth of 10 MHz as compared to a signal of 2 MHz will receive 13dB less

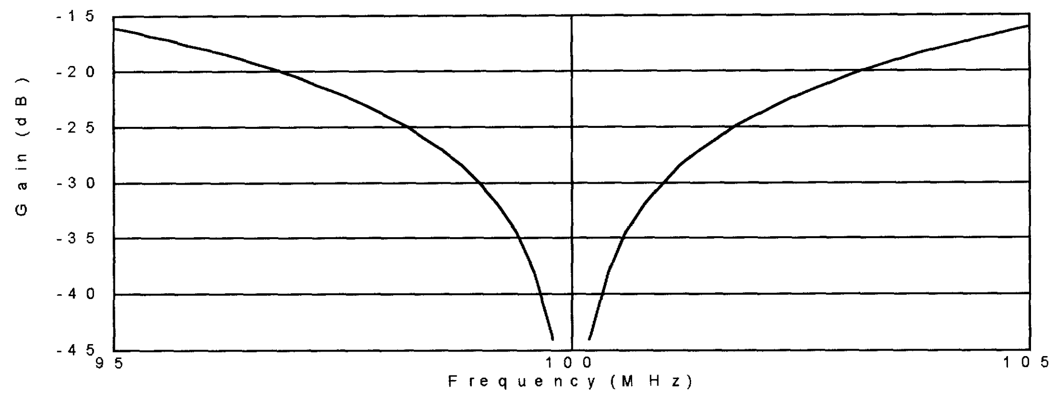

Figure 2.8 Two-element Cancellation Performance.

attenuation at its outer frequencies.

Examining the equation for the output power $|H(\omega)|^2$ more closely, we realize that the depth of the null also increases as the angle of arrival of the interference signal leaves broadside(θ=0°). The output power as the angle of arrival travels from 0-90° for frequencies varying from 1-5 MHz from a center frequency fo = 100 MHz is plotted in Figure 2.9. As we can see, a signal arriving from broadside and 5MHz from the center frequency gets attenuated by only 15 dB. This is because the closer we get to broadside, the smaller the time

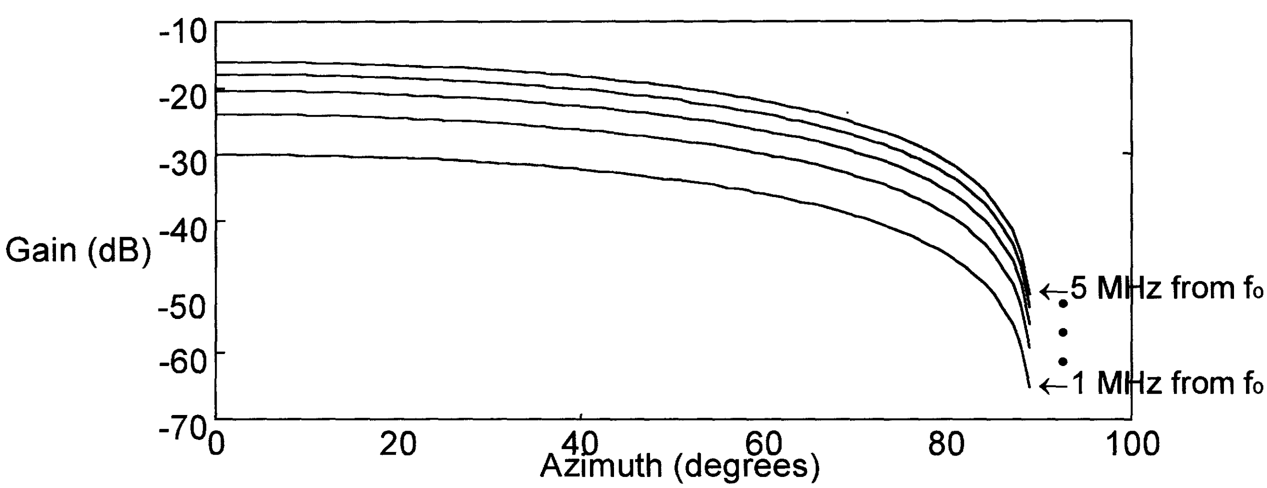

Figure 2.9 Cancellation vs. Arrival Angle for Off-Center Frequencies.

delay the signal experiences between elements and the harder it is too approximate this small delay with complex weights. Figure 2.9 also illustrates the bandwidth degradation discussed and shown in Figure 2.8

2.3.2 Amplitude and Phase Mismatch

Previously, we examined the degradation of interference cancellation due to the effects of interference bandwidth and angle of arrival while assuming that the gain and phase associated with each weight were exact. This, however, is not the case as the weights are represented by a finite number of bits determined by the specific hardware used. Using the previously derived output power $|H(\omega)|^2$ while ignoring the effects of bandwidth and arrival angle, produces a basic model for amplitude and phase mismatch. The interference output power for a two-element array now has the form

$$|H(\omega)|^2 = 1 + a^2 - 2a\cos\phi \qquad \textbf{(2.16)}$$

where the phase error is zero for $\phi=0$, and the amplitude error is zero for a=1. [8] Figure 2.10 shows the corresponding plot of interference cancellation for various amplitude and phase

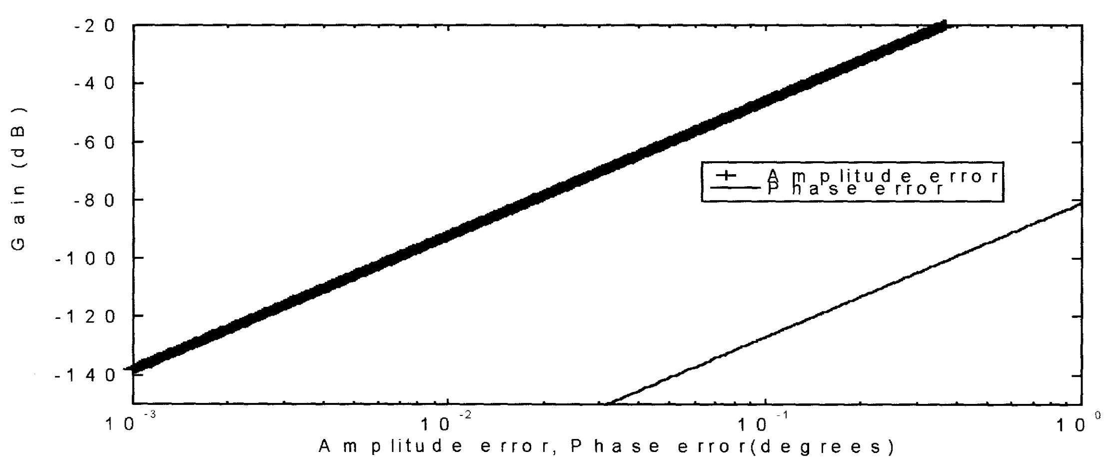

Figure 2.10 Cancellation for Amplitude and Phase Mismatch

---

[8] Phase $\phi = \frac{\omega \Delta z}{c}\sin\theta$

errors in a two-element system. In order to achieve an attenuation of 60dB, the plot indicates that we need an amplitude error of less than .02 and a phase error less than 1°.

2.4 Tapped Delay Lines

As we just observed in Section 2.3, the bandwidth of the interference signal affects the ability of the array to reject such signals. This is due to the fact that the inter-element phase shift ϕ is a function of frequency,

$$\phi = \omega\tau = \frac{\omega \Delta z}{c} \sin\theta . \quad \textbf{(2.17)}$$

Since the phase shift varies across the bandwidth of the interference signal, to achieve perfect cancellation we would need to introduce a new process on each array element. The now standard process, one which uses tapped delay lines, is able to provide a phase shift that could vary with frequency. As in the two-element case in Section 2.3, to achieve perfect cancellation we need

$$w_1 = -w_2 e^{-j\omega\tau} = -w_2 e^{-j\phi} \quad \textbf{(2.18)}$$

where ω corresponds to a single radian frequency ω_o. If we use a tapped delay line as illustrated in Figure 2.11, we arrive at a transfer function which is a function of frequency,

$$H(\omega) = w_1 + w_2 e^{-j\omega\tau} + w_3 e^{-j2\omega\tau} + \ldots w_N e^{-j(N-1)\omega\tau} \quad \textbf{(2.19)}$$

Using this method, we are better able to compensate for the difference in phase shift across frequencies, and thus don't require ω to be a single frequency. Essentially, the tapped delay line, by turning off and on the weights at various points, inserts a variable delay behind each array element. The more taps, the better the approximation to an non-integer delay and the closer we come to placing an exact null on a non-zero bandwidth interference signal.

In typical situations, interference signals are not simply narrowband, but both wideband and narrowband. While tapped delay lines have become the standard approach to dealing with the wideband problem, the method of band-partitioning, to be presented in Chapter 4, addresses the same wideband issue with excellent results.

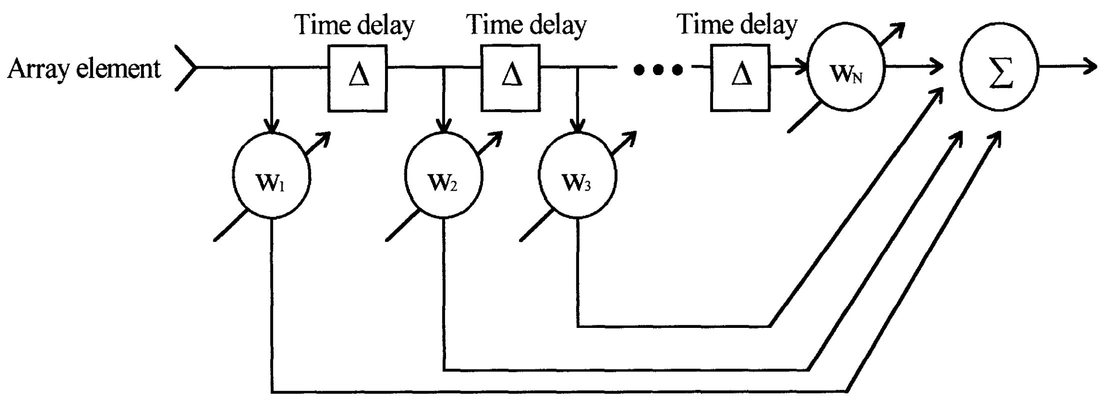

Figure 2.11 Tapped Delay Line with N complex weights.

2.5 Degrees of Freedom

We have previously shown the ability of a two-element array to cancel one interference signal. Revisiting an adaptive array with N elements, a narrowband signal arriving from an angle θ with a radian frequency ω produces an array signal vector of

$$X = e^{j\omega t}\begin{bmatrix}1 & e^{-j\phi_2} & \cdots & e^{-j\phi_N}\end{bmatrix}^T, \qquad \textbf{(2.20)}$$

where ϕi is the phase shift from the first to the ith element. The output signal is then obtained by applying a complex weight to each element and summing the result over all elements. The output signal has the form

$$y(t) = \mathrm{Re}\left\{e^{j\omega t}[w_1 + w_2 e^{-j\phi_2} + \cdots + w_N e^{-j\phi_N}]\right\}. \tag{2.21}$$

Looking closely we see the already visited beampattern response with

$$B(\theta) = w_1 + w_2 e^{-j\phi_2} + \cdots + w_N e^{-j\phi_N}. \tag{2.22}$$

If we wish to place a null at an angle of θ_1, the weights must be chosen so that

$$B(\theta_1) = w_1 + w_2 e^{-j\phi_2(\theta_1)} + \cdots + w_N e^{-j\phi_N(\theta_1)} = 0. \tag{2.23}$$

There are infinite non-zero solutions to this one equation with N unknowns. If, however, we impose a second null at θ_2, the weights must also satisfy the equation

$$B(\theta_2) = w_1 + w_2 e^{-j\phi_2(\theta_2)} + \cdots + w_N e^{-j\phi_N(\theta_2)} = 0. \tag{2.24}$$

Furthermore, we can steer the beam, putting a beam maximum at an angle θ_3. This constraint yields a third equation

$$\left.\frac{dB}{d\theta}\right|_{\theta=\theta_3} = -j\phi_2'(\theta_3) w_2 e^{-j\phi_2(\theta_3)} \cdots - j\phi_N'(\theta_3) w_N e^{-j\phi_N(\theta_3)} = 0. \tag{2.25}$$

Placing a constraint on a beam maximum, or rather steering the beam to where we expect our desired signal to appear, requires only one degree of freedom. Since we have N weights and therefore N unknowns, we can find a non-zero solution for at most N equations. Thus, an N element array can successfully cancel N-1 narrowband interference signals while maintaining a beam maximum in the direction of the wanted signal.

All previous computations in Chapter 2 calculated the weights needed to cancel interference signals by exploiting the fact that we knew the frequency and angle of arrival of the various sources. While this served to demonstrate the ability of an array to realize interference cancellation through complex weight control, it is not a practical approach.

Practical systems cannot be expected to know the number of signals present, their frequency content, and their angle of arrival. This leaves us with the goal of Chapter 3, to develop a practical method to solve for the necessary weights in an adaptive array.

Chapter 3

3. Adaptive Algorithms

An adaptive array attempts to cancel interference signals by adjusting complex weights on each antenna element. Assuming for the moment that the signal environment is stationary, not changing with respect to time, there are two criteria that are most used in communication systems to establish theoretical performance limits of an array. They are the mean-square-error criterion (MSE) and the maximum-likelihood criterion (ML). In Chapter 2 we discussed the constraints imposed by the array itself. Now, let us investigate the methods and adaptive algorithms used in determining the optimal steady-state weights.

3.1 Steady-State Solution for Adaptive Weights

The importance of the steady-state solution derives from the fact that it is this solution that provides the theoretical limits to how well any complex weight algorithm can perform. First, we will investigate the above mentioned criteria and see how they lead to a similar equation for the optimum complex weight solution. Then, in Section 3.2, the least-mean-square (LMS) and direct matrix inversion (DMI) methods for implementing these solutions will be compared.

3.1.1 Mean-Square-Error (MSE) Criterion

The minimum mean-square-error criterion, originally established by Widrow, is based on the standard array configuration in Figure 3.1. Subtracting the array output from the desired signal results in an error signal

$$e(t) = d(t) - y(t)\,. \tag{3.1}$$

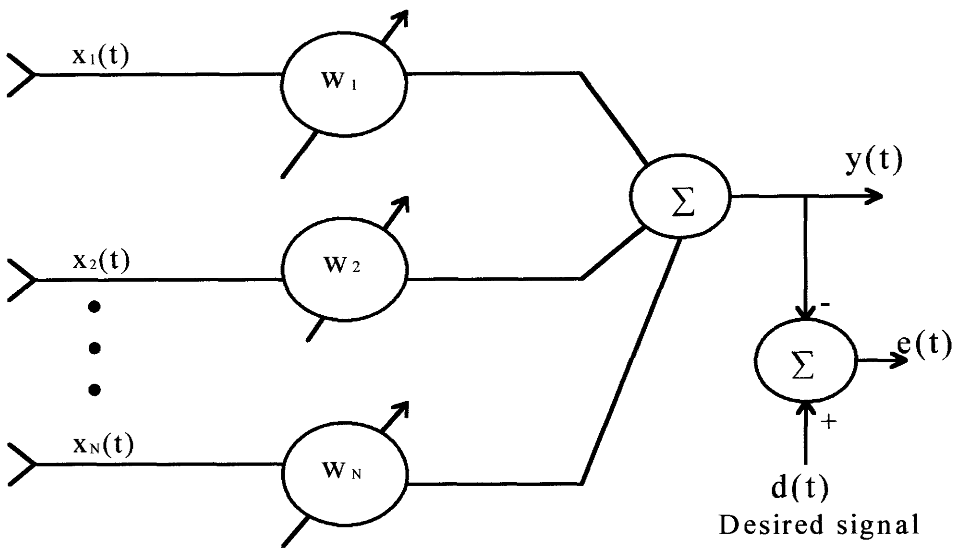

Figure 3.1 Adaptive array structure with known desired signal

To minimize this error signal, the weights are adjusted and optimized. One may question how a system that is privy to the desired communication signal a priori is useful. In practice though, for this system to work, an exact replica of the desired signal is not needed. Rather, d(t) only has to satisfy the constraint that it must be correlated with the communication signal and uncorrelated to the interference signals. In communication systems, which typically use pseudo-noise codes to transmit information, this constraint is met.

Continuing our derivation for the optimal complex weights, if we define y(t) as

$$y(t) = \mathbf{W}^{+}\mathbf{X}(t). \qquad \textbf{(3.2)}$$

where

$$\mathbf{X}(t) = \begin{bmatrix} x_1(t) & x_2(t) & \cdots & x_N(t) \end{bmatrix}^T, \qquad \textbf{(3.3)}$$

the error signal reduces to

$$e(t) = d(t) - \mathbf{W}^{+}\mathbf{X}(t). \qquad \textbf{(3.4)}$$

In order to make the output signal come as close as possible to desired signal, we wish to minimize the squared error between the two signals. The squared error becomes

$$e^2(t) = d^2(t) - 2d(t)\mathbf{X}^T(t)\mathbf{W} + \mathbf{W}^+\mathbf{X}(t)\mathbf{X}^T(t)\mathbf{W}\,. \tag{3.5}$$

Assuming x(t) and d(t) are stationary, we can take the expected value over t. This yields a mean-squared-error

$$E[e^2(t)] = E[d^2(t)] - 2E[d(t)\mathbf{X}^T(t)]\mathbf{W} + \mathbf{W}^+E[\mathbf{X}(t)\mathbf{X}^T(t)]\mathbf{W}\,. \tag{3.6}$$

Using the definition of auto-correlation, where

$$\mathbf{R}_{xx} = E[\mathbf{X}(t)\mathbf{X}^T(t)] = \begin{bmatrix} E[x_1(t)x_1(t)] & E[x_1(t)x_2(t)] & \cdots & E[x_1(t)x_N(t)] \\ E[x_2(t)x_1(t)] & E[x_2(t)x_2(t)] & \ldots & \cdots \\ \vdots & \vdots & & \vdots \\ E[x_N(t)x_1(t)] & \cdots & \ldots & E[x_N(t)x_N(t)] \end{bmatrix} \tag{3.7}$$

and

$$\mathbf{r}_{dx} = E[d(t)\mathbf{X}^*(t)] = \begin{bmatrix} E[d(t)x_1^*(t)] \\ E[d(t)x_2^*(t)] \\ \vdots \\ E[d(t)x_N^*(t)] \end{bmatrix} \tag{3.8}$$

we can express the mean-square-error in a more convenient notation. Equation 3.6 now becomes

$$E[e^2(t)] = E[d^2(t)] - 2\mathbf{r}_{dx}\mathbf{W} + \mathbf{W}^+\mathbf{R}_{xx}\mathbf{W}\,. \tag{3.9}$$

Furthermore, if we define $E[d^2(t)]$, which is the power of our desired signal, as equal to S, Equation 3.9 simplifies to

$$E[e^2(t)] = S - 2\mathbf{r}_{dx}\mathbf{W} + \mathbf{W}^{+}R_{xx}\mathbf{W}\,. \tag{3.10}$$

We can see from the above expression that the mean-square error is a quadratic function of the weights. Since the square error must be a positive quantity and increasing the weight vector increases the square error, the quadratic surface must be concave up and have a defined global minimum. This is an important result and implies that the optimal set of weights that minimize the square error correspond to the point on the bottom of the bowl-like quadratic surface. By differentiating $E[e^2(t)]$ with respect to the weight vector and setting the gradient equal to zero,

$$\nabla_w\{E[e^2(t)]\} = \frac{\partial E[e^2(t)]}{\partial \mathbf{W}^{+}} = 0 \tag{3.11}$$

we obtain the equation

$$\nabla_w\{E[e^2(t)]\} = 0 = -2\mathbf{r}_{dx} + 2\mathbf{R}_{xx}\mathbf{W}\,. \tag{3.12}$$

It follows that the optimal weight vector, assuming $\mathbf{R}$ is nonsingular so that $\mathbf{R}^{-1}$ exists, is found to be

$$\mathbf{W}_{opt} = \mathbf{W}_{MSE} = \mathbf{R}_{xx}{}^{-1}\mathbf{r}_{dx}\,. \tag{3.13}$$

This vector can be simplified even further if our wanted communications signal s(t), incident on the array, is a single signal source with $s(t) = e^{j\omega_o t}$. The signal vector $\mathbf{S}(t)$ is then

$$\begin{aligned}\mathbf{S}^T(t) &= e^{j\omega_o t}[1, e^{-j\phi_2}, \ldots e^{-j\phi_N}] \\ &= s(t)v^T\end{aligned}\,. \tag{3.14}$$

where

$$\mathbf{v}^T = [1, e^{-j\phi_2}, \ldots e^{-j\phi_N}]. \tag{3.15}$$

Using (3.14), the array input vector $\mathbf{X}(t)$ can be written as

$$\mathbf{X}(t) = s(t)\mathbf{v} + \mathbf{N}(t) \tag{3.16}$$

where $\mathbf{N}(t)$ represents the noise vector due to interference signals. Since the desired signal and the noise due to the interference signals are uncorrelated, the expected value of the product of the two should equal zero. Furthermore, our desired signal should be correlated with our communications signal s(t), and the expected value of these two quantities should equal the power of the communications signal to within a constant. With this in mind,

$$\mathbf{r}_{dx} = E[d(t)\mathbf{X}^*(t)] \tag{3.17}$$

$$= E[d(t)(s^*(t)\mathbf{v}^* + \mathbf{N}^*(t))]$$

$$= E[d(t)s^*(t)\mathbf{v}^* + d(t)\mathbf{N}^*(t)]$$

$$= E[d(t)s^*(t)\mathbf{v}^*]$$

$$\mathbf{r}_{dx} = S\mathbf{v}^* \tag{3.18}$$

where S, as defined earlier, is the power of the desired signal. The optimal weights from (3.13) are now simply

$$\mathbf{W}_{opt} = \mathbf{W}_{MSE} = S\mathbf{R}_{xx}^{-1}\mathbf{v}^* \tag{3.19}$$

where v is the steering vector, the direction vector in which we expect our desired signal. This weight vector in (3.19), often referred to as the Wiener solution, corresponds to the point on the quadratic surface representing the minimum mean-square error (MSE).

Finally, using matrix properties where $[AB]^T=B^TA^T$ and $R^+=R$, the MSE equation from (3.10) becomes

$$E_{\min}[e^2(t)] = S - \mathbf{r}_{dx}{}^{+}\mathbf{R}_{xx}{}^{-1}\mathbf{r}_{dx}\,. \tag{3.20}$$

3.1.2 Maximum-Likelihood

Using the array configuration in Figure 3.1, but now assuming that the desired signal structure is completely unknown, leads us to a second criterion for weight optimization. This method, known as the maximum-likelihood method, requires only that the noise has Gaussian statistics. The goal of this criterion is to estimate the parameters which maximize the probability that the output of the array only corresponds to the desired signal and not the noise caused by interference signals. Revisiting (3.16), the array signal vector X(t) can be represented as

$$\mathbf{X}(t) = s(t)\mathbf{v} + \mathbf{N}(t)\,, \tag{3.21}$$

where

$$\mathbf{v}^T = [1, e^{-j\phi_2}, \ldots e^{-j\phi_N}]\ . \tag{3.22}$$

As in the MSE method, we need an estimate of the desired signal s(t). Specifically, we want to estimate s(t) such that the probability density function for $\mathbf{X}(t)$ given (3.21),

$$P\{\mathbf{X}(t) | \mathbf{X}(t) = s(t)\mathbf{v} + \mathbf{N}(t)\} \tag{3.23}$$

is maximized. To simplify our calculations, we can take the negative natural logarithm of (3.23), known as the likelihood function:

$$L[\mathbf{X}(t)] = -\ln[P\{\mathbf{X}(t) | \mathbf{X}(t) = s(t)\mathbf{v} + \mathbf{N}(t)\}]\,. \tag{3.24}$$

Assuming $\mathbf{X}(t)$ is stationary and $\mathbf{N}(t)$ is a vector of Gaussian random variables with a covariance matrix of $\mathbf{R}_{nn}$, (3.24) can be written as follows:

$$L[\mathbf{X}(t)] = [\mathbf{X}(t) - s(t)\mathbf{v}]^{+}\mathbf{R}_{nn}^{-1}[\mathbf{X}(t) - s(t)\mathbf{v}]. \qquad \textbf{(3.25)}$$

The derivation is left in reference [4]. To maximize (3.25), we wish to find a estimate of s(t) such that the derivative of (3.25) with respect to s(t) is zero,

$$\frac{\partial L[\mathbf{X}(t)]}{\partial s(t)} = -2\mathbf{v}^{+}\mathbf{R}_{nn}^{-1}\mathbf{X} + 2\hat{s}(t)\mathbf{v}^{+}\mathbf{R}_{nn}^{-1}v = 0. \qquad \textbf{(3.26)}$$

Solving for the estimated s(t), we obtain

$$\hat{s}(t) = \frac{\mathbf{v}^{+}\mathbf{R}_{nn}^{-1}}{\mathbf{v}^{+}\mathbf{R}_{nn}^{-1}\mathbf{v}}\mathbf{X}(t) = \mathbf{W}_{ML}^{T}\mathbf{X}(t). \qquad \textbf{(3.27)}$$

Thus, the maximum likelihood optimal weight vector is

$$\mathbf{W}_{ML} = \frac{\mathbf{R}_{nn}^{-1}\mathbf{v}^{*}}{\mathbf{v}^{+}\mathbf{R}_{nn}^{-1}\mathbf{v}}. \qquad \textbf{(3.28)}$$

Comparing the weight solution of the mean squared error method in (3.18) to the weight solution of the maximum likelihood method (3.28), we realize that the two are very similar. If we rewrite (3.19) and (3.28) using

$$\mathbf{R}_{xx} = \mathbf{R}_{ss} + \mathbf{R}_{nn}, \quad N_o = \mathbf{W}^{+}\mathbf{R}_{nn}^{-1}\mathbf{W}, \text{ and } \quad S_o = \mathbf{W}^{+}\mathbf{R}_{nn}^{-1}\mathbf{W} = SN_o \qquad \textbf{(3.29)}$$

where N_o and S_o are the noise and signal power, respectively, output from the array,

after several complex matrix manipulations we arrive at:

$$\mathbf{W}_{MSE} = \frac{S_o}{N_o(S_o + N_o)}\mathbf{R}_{nn}^{-1}\mathbf{v}^{*} \qquad \text{and} \qquad \mathbf{W}_{ML} = \frac{1}{N_o}\mathbf{R}_{nn}^{-1}\mathbf{v}^{*}. \qquad \textbf{(3.30)}$$

Surprisingly, the two weight solutions differs only by a scale factor.

3.2 Gradient-Based Algorithms for Adaptive Weights

We have just seen that for a steady-state system, the weights that achieve optimal interference cancellation are directly related to $\mathbf{R}_{xx}^{-1}\mathbf{v}^*$. For such a stationary system, in which the signal environment is unchanging but the signal statistics are unknown, the correlation matrix is determined by taking samples at the N array elements over an extremely long period of time. The resulting array input vector , $\mathbf{X}(t)$, is then used to compute the correlation matrix:

$$\mathbf{R}_{xx} = E[\mathbf{X}(t)\mathbf{X}^*(t)], \text{ for t=0-}\infty. \tag{3.31}$$

Finally, the weights are computed by taking the inverse of (3.31) and multiplying by the steering vector.

Unfortunately, in most applications the signal environment does change over time and thus taking an infinite number of samples in order to find the true correlation matrix is not feasible. After taking samples and computing the optimal weights, the signal environment would have changed and the current optimal weights would be different from the ones computed. Essentially, the computed weights would be worthless.

So, we are left with the problem of developing an algorithm for the weights that converges as quickly as possible to the optimal weights. Let us investigate two adaptive algorithm that attempt to do just that , the least mean square (LMS) and the direct matrix inversion (DMI) algorithms.

3.2.1 Least Mean Square (LMS)

The least mean square algorithm is by far the most widely used algorithm for converging to the optimal weights solution. This algorithm, based on a gradient search method, is extremely applicable to quadratic performance surfaces. Since quadratic surfaces have an absolute minimum, the gradient method uses a gradient estimate (slope estimate) to determine the direction of the performance surface minimum.

3.2.1.1 Gradient Search Method

Let us review the derivation of the MSE in Section 3.1 to illustrate its quadratic nature. As we recall, the error signal, the difference between the desired signal and array output, was expressed as

$$e(t) = d(t) - \mathbf{W}^{+}\mathbf{X}(t). \tag{3.32}$$

In order to make the output signal come as close as possible to the desired signal, we wished to minimize the squared error between the two signals:

$$e^2(t) = d^2(t) - 2d(t)\mathbf{X}^T(t)\mathbf{W} + \mathbf{W}^{+}\mathbf{X}(t)\mathbf{X}^T(t)\mathbf{W}. \tag{3.33}$$

Assuming x(t) and d(t) were stationary, we took the expected value over t. This yielded a mean squared error

$$E[e^2(t)] = E[d^2(t)] - 2E[d(t)\mathbf{X}^T(t)]\mathbf{W} + \mathbf{W}^{+}E[\mathbf{X}(t)\mathbf{X}^T(t)]\mathbf{W}. \tag{3.34}$$

which we expressed in a more convenient notation as

$$E[e^2(t)] = S - 2\mathbf{r}_{dx}\mathbf{W} + \mathbf{W}^{+}\mathbf{R}_{xx}\mathbf{W}. \tag{3.35}$$

As seen earlier, the mean square error of (3.35) is a quadratic function in terms of the weight vector. Thus, we can use a gradient approach to find the optimal weights that cause the mean-square error to be minimized.

Not knowing the location of the minimum of the performance surface, the gradient search algorithm begins with a guess of the optimal weight vector. Then, an estimate of the gradient vector, or slope of the curve, at this point is measured and a new weight vector is computed. Since the gradient is in the direction of steepest upward slope, the new weight vector is chosen equal to the previous guess minus some increment proportional to the direction of the gradient. The process repeats until eventually the optimal weights are reached. The iterative search method has the form:

$$\mathbf{W}_{k+1} = \mathbf{W}_k - \mu\nabla_k \tag{3.36}$$

where k is the iteration number, $\mathbf{W}_k$ is the current weight vector, and μ is the step size.

While the step size is chosen so that $0<\mu<1$, typically, the smaller the step size the closer we get to the optimal weights, but the longer it takes to get there.

3.2.1.2 LMS Derivation

The LMS algorithm uses (3.36) where at any iteration k, the gradient of $e^2(k)$ is chosen as the estimated gradient. The weight vector algorithm now becomes

$$\mathbf{W}_{k+1} = \mathbf{W}_k - \mu\nabla[e^2(k)]. \tag{3.37}$$

The estimated gradient of a single time sample is

$$\hat{\nabla}_k = \nabla[e^2(k)] = \begin{bmatrix} \frac{\partial e^2(k)}{\partial w_o} \\ \vdots \\ \frac{\partial e^2(k)}{\partial w_N} \end{bmatrix} = 2e(k)\nabla[e(k)]. \tag{3.38}$$

Remembering (3.32) but replacing t with k,

$$e(k) = d(k) - \mathbf{W}^{+}\mathbf{X}(k) \tag{3.39}$$

and thus the gradient of e(k) with respect to the weights reduces to

$$\nabla[e(k)] = \nabla[d(k) - \mathbf{W}^{+}\mathbf{X}(k)] = -\mathbf{X}(k)\,. \qquad \textbf{(3.40)}$$

Plugging (3.40) into (3.38), the estimated gradient can be written as:

$$\hat{\nabla}_k = -2e(k)\mathbf{X}(k)\,. \qquad \textbf{(3.41)}$$

Finally, substituting (3.41) into the weight algorithm of (3.37), we arrive at the least mean square weight vector algorithm:

$$\mathbf{W}_{k+1} = \mathbf{W}_k + 2\mu e(k)\mathbf{X}(k)\,. \qquad \textbf{(3.42)}$$

Since (3.42) requires no averaging, differentiation, or squaring, the LMS algorithm is extremely simple and efficient to implement. This strength accounts for the popularity of the LMS algorithm.

3.2.1.3 Transient Response of LMS

It can be shown that the transient response of the LMS weights, or rather the speed of the convergence to the optimal weights, is determined by time constants of the form:

$$\tau_p = \frac{1}{2\mu\lambda_p}\,,\ \text{p=1,2,...,N} \qquad \textbf{(3.43)}$$

where λ_p is the p$^{\text{th}}$ eigenvalue or signal power of the correlation matrix $\mathbf{R}_{xx}$. Since the transient response of the LMS algorithm is determined by the smallest signal power and the choice of step size μ, it is often difficult to choose an appropriate step size. To approach as close as possible to the optimal weights, we want a small step size. However, if the signal environment is changing, we want to approach the optimal weight as quick as possible, which according to (3.43) requires a large step size.

The appropriate step size, the smallest one which would still allow a specific transient response to be met, could be chosen if we knew the smallest signal power (eigenvalue). Of course this is not known, and thus the convergence time of the LMS algorithm is very susceptible to differences in interference signal powers, also known as the eigenvalue spread. While the LMS algorithm is extremely easy to implement, the transient problem due to eigenvalue spread, leads us to our second algorithm, direct matrix inversion.

3.2.2 Direct Matrix Inversion (DMI)

In many practical applications, either the signal environment changes quickly or the platform on which the array is placed is in constant motion. In both situations, the ability of the array to reject interference signals is completely reflected by the convergence rate of the adaptive algorithm used. Where the speed of convergence to the optimal steady-state weight solution is imperative, an algorithm that is insensitive to eigenvalue spread is of valued importance. Direct matrix inversion is such an algorithm.

3.2.2.1 DMI Derivation

Direct matrix inversion simply approximates the optimal weight solution

$$\mathbf{W}_{opt} = \mathbf{R}_{xx}^{-1}\mathbf{r}_{dx} = \mathbf{R}_{xx}^{-1}\mathbf{v}^{*} \tag{3.44}$$

by estimating $\mathbf{R}_{xx}$ over a finite observation interval. In communication systems, the desired signal is often many orders of magnitude smaller than the interference signals and typically close to the thermal noise of the actual receiver. Whether this is the case, or the weights are adjusted over intervals when the desired signal is known to be absent, the estimated correlation matrix $\mathbf{R}_{xx}$ becomes $\mathbf{R}_{nn}$. Thus, the estimated covariance matrix is

$$\hat{\mathbf{R}}_{xx} = \hat{\mathbf{R}}_{nn} = \frac{1}{K}\sum_{i=1}^{K}\mathbf{X}(i)\mathbf{X}^{+}(i) \tag{3.45}$$

where $\mathbf{X}$(i) is the i[th] time sample of array input vector $\mathbf{X}$(t). Earlier, we defined the output of the array as $y(t) = \mathbf{W}^T[\mathbf{S}(t) + \mathbf{N}(t)]$. Noting that the output power of the desired signal only is

$$E\{|y_s(t)|^2\} = |\mathbf{W}^T\mathbf{S}|^2 \tag{3.46}$$

while the output noise power is

$$E\{|y_n(t)|^2\} = |\mathbf{W}^T\mathbf{N}|^2 \tag{3.47}$$

gives us a signal to noise ratio (SNR) of

$$\left(\frac{s}{n}\right) = \frac{E\{|y_s(t)|^2\}}{E\{|y_n(t)|^2\}} = \frac{|w^T\mathbf{S}|^2}{|w^T\mathbf{N}|^2} = \frac{\mathbf{W}^T[\mathbf{S}\mathbf{S}^T]\mathbf{W}}{\mathbf{W}^T[\mathbf{N}\mathbf{N}^T]\mathbf{W}}\ . \tag{3.48}$$

If we normalize (3.48) by the maximum SNR, So/No ,

$$\sigma = \frac{(s/n)}{(S_o/N_o)} \tag{3.49}$$

where σ is a measure of how close we come to the optimal SNR. The probability distribution of (3.49) formulated using the incomplete Beta distribution described in [5] [6] is

$$\Pr(\sigma \le q) \cong \frac{K!}{(N-2)!(K+1-N)!}\int_0^1 (1-u)^{N-2}u^{K+1-N}du \tag{3.50}$$

where N is the number of adaptive weights, and K is the number of time samples used to estimate $\mathbf{R}_{nn}$.

3.2.2.2 DMI Transient Response

Using the properties of the Beta distribution, from (3.50) we can compute the expected value and variance of σ. Dependent on K and N, the expected value of σ is

$$E(\sigma) = \frac{K - N + 2}{K + 1} \tag{3.51}$$

while the variance is

$$\mathrm{var}(\sigma) = \frac{(K - N + 2)(N - 1)}{(K + 1)^2 (K + 2)} . \tag{3.52}$$

Looking closely at (3.52), we observe an amazing result. The variance is completely independent of the spread of the eigenvalues.[9] Computing the optimal weights by estimating the covariance matrix has eliminated the problem encountered by the LMS algorithm. The number of samples needed to compute an effective covariance matrix can be determined by plotting (3.51). To come within 60% (~3dB) of the maximum SNR, it is apparent from Figure 3.2 that the covariance matrix should be formed by using a number of time samples greater than two times the number of antenna elements. Considering the number of time

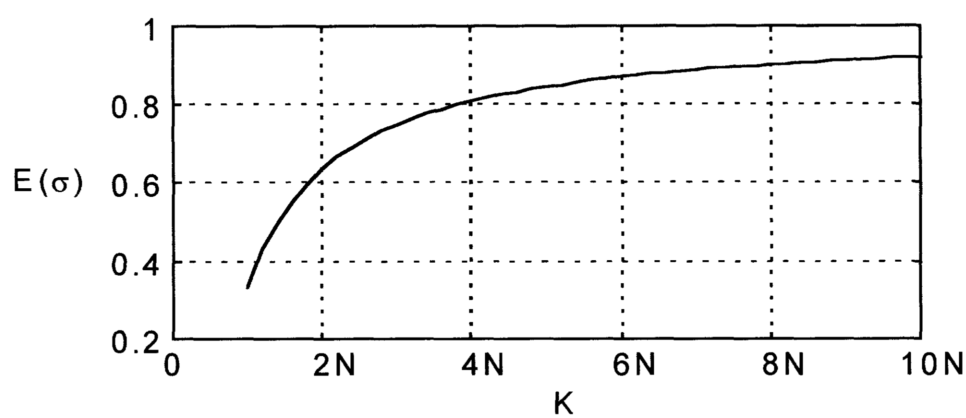

Figure 3.2 E(σ) vs. K for N≥2

[9] In actuality, as illustrated in [4], if less than 10 bits are used when computing the inverse covariance matrix, var(σ) is slightly dependent on the eigenvalue spread.

samples needed to compute the weights gives us a bound on the transient nature of both the LMS and DMI algorithm.

While the complex weights necessary in a five element adaptive array require only 10 time samples by direct matrix inversion, the LMS algorithm could require anywhere from 10 to several hundred time samples due to eigenvalue spread. Even though direct matrix inversion has its clear advantage over the LMS algorithm when it comes to rapid convergence to steady-state, until recently, it has not been utilized. This can be accounted for by the fact that DMI requires far more complex circuitry than does the LMS algorithm. Estimating $\mathbf{R}_{xx}$ when using DMI requires KN(N+1)/2 complex multiplications. In addition , inverting $\mathbf{R}_{xx}$ requires $(N^3/2+N^2)$ complex multiplications and computing the weights another N^2 multiplications.

The LMS algorithm can be implemented completely through simple analog techniques with minimal hardware. Unfortunately, with this simplicity comes limitations. Enhancements for improved performance in an analog system are extremely difficult once the system is built. In a digital system, however, algorithms can be modified very easily. Furthermore, a digital system allows for the use of fast adapting algorithms such as direct matrix inversion.

Due to staggering advances in computer technology over the last 3-4 years, it is now possible to perform computationally intensive complex algorithms that require high speed digital processing. This new ability, in combination with the ability to efficiently implement the discrete fourier transform by computer, has initiated the investigation of new advanced adaptive array algorithms that were before impractical. This leads us Chapter 4, the exploration of an improved interference cancellation technique called adaptive band-partitioning.

Chapter 4

4. Adaptive Band-Partitioning Approach

In Chapter 2 we observed how the introduction of complex weights to an array could increase the array's ability to reject interference signals. We then investigated the severe drawback of the traditional method, bandwidth degradation. Adaptive band-partitioning attempts to address and alleviate such dependence on interference bandwidth by utilizing digital techniques including the Fast Fourier Transform and direct matrix inversion.

4.1 Adaptive Algorithm

The traditional method for interference cancellation attempts to approximate a time delay through multiplication of a single complex weights on each array element. As illustrated in Figure 2.7 and derived in Section 2.3, if we have a two-element array, the output y(t) has the form

$$y(t) = w_1 n(t) + w_2 n(t-\tau). \qquad \textbf{(4.1)}$$

Taking the Fourier transform, the frequency domain representation, assuming the interference signal is stationary, is

$$Y(\omega) = N(\omega)[w_1 + w_2 e^{-j\omega\tau}]. \qquad \textbf{(4.2)}$$

If the signal n(t) were a narrowband signal with a center frequency of f_o, ω would equal ω_o and we would thus be able to perfectly cancel the signal by choosing

$$w_1 = -w_2 e^{-j\omega_o\tau}. \qquad \textbf{(4.3)}$$

For situations in which interference signals are not narrowband, the bandwidth of the signal greatly affects the ability of the array to reject such signals.

We discovered that this was due to the fact that the inter-element phase shift ϕ was a function of frequency,

$$\phi = \omega\tau = \frac{\omega \Delta z}{c}\sin\theta . \tag{4.4}$$

Since the phase shift varies across the bandwidth of the interference signal, to achieve perfect cancellation we observed that we would need to introduce a new process, one which could apply a phase shift that varied with frequency.

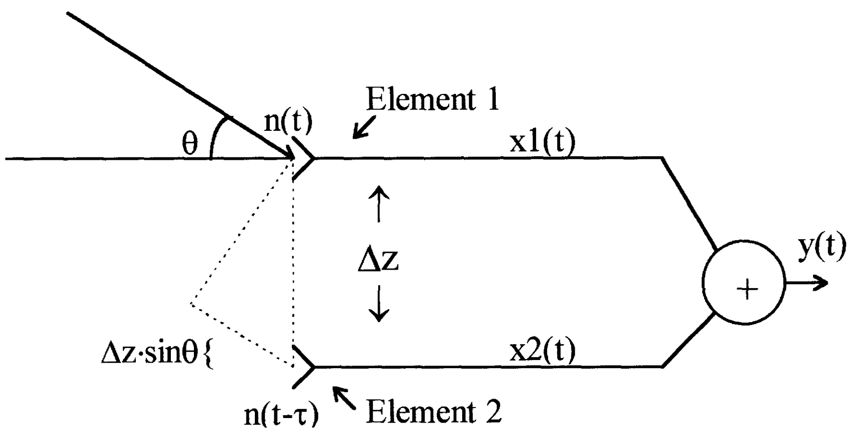

Figure 4.1 Classical Two-element array

Let us take a step back and look at Figure 2.7 but without the weights. From Figure 4.1 an interference signal n(t) arriving at element 1 at an angle θ arrives at element 2 as a shifted version of itself, n(t-τ). If we assume the signal has a non-zero bandwidth, the Fourier transform of x1(t) and x2(t) is

$$x1(f) = N(f) \text{ and } x2(f) = N(f)e^{-j2\pi f\tau} \tag{4.5}$$

The most obvious method of canceling the signal would be to multiply x2(f) by $e^{j2\pi f\tau}$ and subtract this from x1(f). Notice, multiplying x2(f) by $e^{j2\pi f\tau}$ is essentially multiplying each frequency f in x2 by a complex number. Amazing, by performing this in the frequency domain where the correct weight is applied to each individual frequency, we have perfect cancellation for an interference signal with a bandwidth.

To multiply each frequency by a complex number, we would need a complex weight for each frequency. Of course it is not practical to place a complex weight on each frequency, but we can place weights on a large number of frequencies or frequency bins. Essentially, we can partition a frequency band of interest into smaller bins and apply weights to each of these bins. The result is our adaptive band-partitioning algorithm:

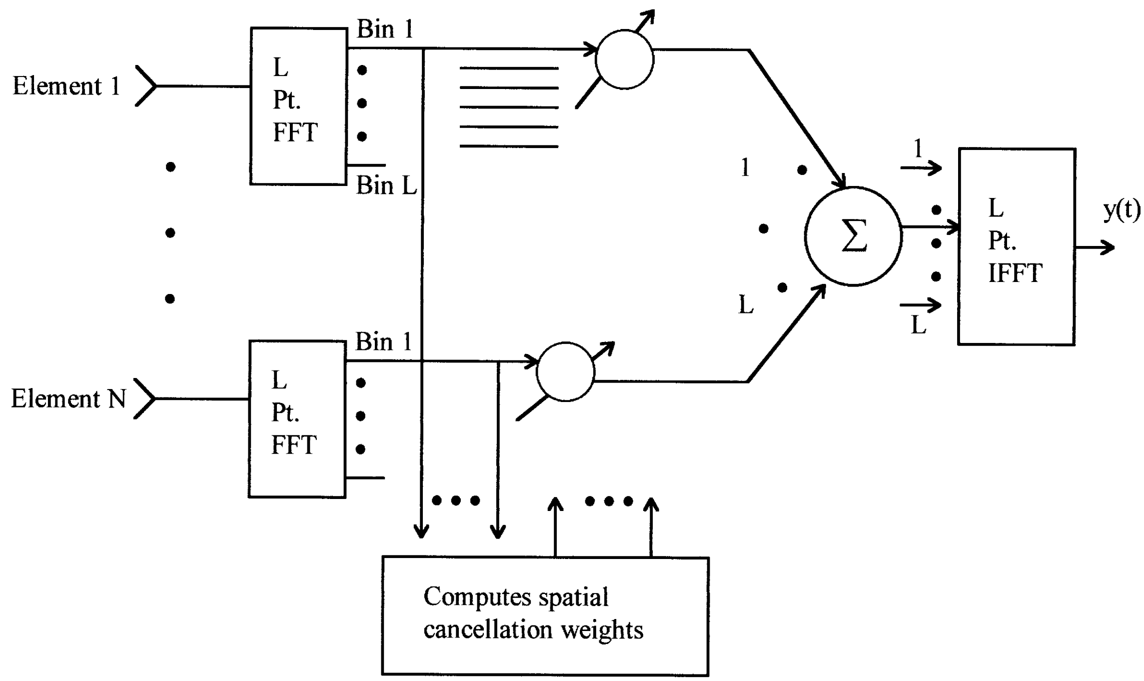

Figure 4.2 Adaptive Band-Partitioning Approach

First, a L-point FFT is performed on each of N array elements, dividing the frequency response of each element into L distinct bins. Then, complex weights are applied to each frequency bin of each element. Where in the classical adaptive array we applied one complex weight to each element, the new approach places L weights on each element, corresponding to the L frequency bins. To find the optimal weights to cancel an interference signal, we now compute an optimal set of weights separately for each frequency bin. If we define the weight vector for bin 1 as

$$\mathbf{w}_1 = \begin{bmatrix} w_{11} \\ \vdots \\ w_{1N} \end{bmatrix} \tag{4.6}$$

and the vector of frequencies for bin 1 as

$$\mathbf{f}_1 = \begin{bmatrix} f_{11} \\ \vdots \\ f_{1N} \end{bmatrix} \tag{4.7}$$

the output frequency for bin 1 is

$$f_{1out} = \mathbf{w}_1{}^T \mathbf{f}_1 . \tag{4.8}$$

Taking the output frequency for each of L bins and then computing the L-point IFFT gives us our output signal y(t), hopefully now devoid of all interference signals.

Whereas the N-element classical array was capable of canceling N-1 narrowband interference signals while steering the array toward the desired signal, adaptive band-partitioning has the ability of canceling N-1 narrowband interference signals in each of L frequency bins. Furthermore, cancellation is no longer dependent on interference bandwidth. Since we are applying adaptive weights to each frequency, a wideband interference signal can be completely cancelled. The performance of adaptive band-partitioning under various circumstances is simulated in Section 4.4.

4.2 Applying DMI

To compute the weights necessary for each frequency bin, the DMI algorithm of Chapter 3, Section 3.2.2 is used. As determined by Figure 3.2, to obtain a reasonable estimate of $\mathbf{R}_{xx}$ we need to take at least 2N time samples per array element. Instead, since we are now dealing with deriving weights in the frequency domain, for each array element we need to average at least 2N samples for each frequency bin. This leads to taking quite a few more time samples than in the classical case. If we average 2N consecutive segments of L time samples overlapped by 50%, we arrive at

$$\begin{aligned} \text{no. time samples} &= \text{fftsize} + (\text{fftsize-overlap})2N \\ &= L+(L/2)2N \\ &= L(N+1) \quad \text{for } 50\% \text{ overlap.} \end{aligned} \tag{4.9}$$

While the number of time samples might seem excessive, in communication systems that have bandwidths of 10-25 MHz, and thus sampling rates of 20 MHz and higher, the associated time delay is not a concern. This will become obvious in the simulation which follows.

4.3 Simulation Setup

To confirm and further characterize the ability of the adaptive band-partitioning algorithm to reject narrowband and wideband interference signals, extensive simulations were performed on various interference environments. To approximate a communication system, a bandwidth of 25 MHz set on a carrier frequency of 1.4 GHz was chosen.

4.3.1 Array Configuration

For comparison purposes and ease of implementation, the well-studied uniform array with an element spacing of $\lambda/2$ was chosen for all the experiments. Since $\lambda = \dfrac{c}{f_o}$ where f_o is the carrier frequency of 1.4 GHz, we have an inter-element spacing of .107 meters. As each additional array or antenna element introduces a significant cost to the system, often several to tens of thousands of dollars for military applications, a 5-element array was used to simulate a small and affordable array.

4.3.2 Communication Assumptions

Several assumptions were made to make the simulations reasonable and applicable to satellite communication systems. The array was placed along a horizontal axis and phased and oriented to point skyward. Thus, to steer the antenna toward the desired signal sent by the satellite, we need to steer the array to 0°(essentially no steering is needed). In addition, since the only signals that can propagate from directly above are signals sent by satellites, and the main beam width for a 5 element array given by (2.9) is $\pm 17°$, we will assume that interference signals will not be present in the main beam.

There is one other very important assumption we will need to make. Typical communication systems use a method of spread-spectrum coding, often called pseudo-noise coding, to spread their narrowband signal over a wide bandwidth. The purpose of such a technique is to be able to send a signal with much smaller power density, and then correlate the signal at the receiver with a known reference signal to achieve amplification. Since the pseudo-noise code is designed to be uncorrelated with noise, only amplification of the signal is achieved. The important implication of using such a technique is that the amplitude of the desired signal at the receiver, array element, is comparable to the thermal noise level of the receiver. Assuming that the interference signals have large amplitudes compared to the thermal noise level , the system will place nulls only at the location of the largest signals, consequently the interference signals. Thus, when deriving weights to cancel the interference signal, the desired signal will not be mistaken as a large amplitude signal needing rejection. Of course, since we will actually steer the array toward the known location of the desired signal, the desired signal would never be canceled. If the desired signal was, however, much greater in amplitude that the thermal noise, the convergence rate of the weights would be much slower. Consequently, the 2N frequency samples needed by the DMI algorithm would not be enough to derive sufficient weights and achieve interference cancellation.

4.3.3 Convergence Rate

As stated earlier, the convergence rate of an adaptive algorithm is critical if the signal environment is rapidly changing or the platform on which the array is placed is in motion. Let us examine the actual time required by the DMI algorithm in our simulated communication scenario using adaptive band-partitioning. If we choose to compute 2N blocks of 256-point FFTs overlapping each block by 50%, we need L(N+1) time samples, (4.9). Having chosen L=256 and 5 elements, this requires us to take 1536 time samples. Since our communications bandwidth of 25 MHz requires a sampling rate of 50 MHz, we have a time sample every 1/50MHz or rather every 20ns. Thus, our convergence rate, the time for our algorithm to converge, is

$$1536 \text{ time samples } \times \text{ } 20\text{ns/sample} = 30.7\mu\text{sec.} \qquad \textbf{(4.10)}$$

To see how robust this seemingly small time is, let us imagine that the array is on a platform, such as a plane, moving at 500miles/hr.. Converting this speed to inches/μsec we have

$$500\frac{miles}{hour}\times\frac{1hour}{60\,\text{min.}}\times\frac{1\,\text{min.}}{60\,\text{sec.}}\times\frac{1\,\text{sec.}}{10^6\,\mu\,\text{sec}}\times\frac{5280ft.}{1mile}\times\frac{12inches}{1ft.}=.0088\frac{inches}{\mu\,\text{sec}}.$$

Multiplying this result by the convergence rate of (4.10), the plane will move only

$$30.7\,\mu\,\text{sec}\times.0088\frac{inches}{\mu\,\text{sec}}=.27inches$$

in the time it takes the algorithm to converge. This movement is extremely small and would lead to the array moving less than a degree off axis. Thus, in our test scenario the convergent rate of adaptive band-partitioning algorithm while using DMI is more than adequate.

4.3.4 Jammer Simulation

Two types of interference signals were used to test the adaptive array, narrowband and wideband signals. While narrowband signals were given a bandwidth of 100 kHz, wideband signals were given a bandwidth of 25 MHz, in order to span the entire communication spectrum. To simulate the arrival angle for each interference signal at each of the 5 elements, the signal vector X(t) was generated by delaying the signal appropriately:

$$\mathbf{X}(t) = \begin{bmatrix} x_1(t) \\ \vdots \\ x_N(t) \end{bmatrix}_{N=5} = \begin{bmatrix} s(t) \\ \vdots \\ s(t-(N-1)\tau) \end{bmatrix}_N \quad \text{where } \tau = \frac{\Delta z}{c}\sin\theta = \frac{\lambda}{2c}\sin\theta \qquad \textbf{(4.11)}$$

Finally, the signal vector for each interference signal was added to arrive at the resulting interference vector.

4.4 Simulation Results

The sections to follow each deal with distinct simulations involving a combination of narrowband and wideband interference signals. The desired signal will always be placed at 0° azimuth and will have a power density equal to that of the thermal noise. To set a reference, the thermal noise at each receiver will have a power of 0dB. Hence, an interference signal with a power of 60dB is 60dB above the thermal noise power.

For each scenario, several plots will be included to illustrate the success of adaptive band-partitioning in canceling the interference signals. The first plot will always indicate the location and frequencies of the generated interference signals. The second plot will show the beampattern resulting from the optimal derived weights. The comparison of the two should illustrate the ability of the algorithm to locate the interference signal's frequencies and angle of arrival. The third plot will graph the residual interference power left in each frequency bin after adaptive band-partitioning . Inspecting the residual power left in each frequency bin will give us a final assessment of the success of interference cancellation.

4.4.1 Single Narrowband Interference Signal

Let us first look at the cancellation achieved for narrowband interference signals only. Figures 4.3 to 4.5 were generated for a 60dB interference signal arriving at an angle of -30° and centered at 15MHz. The true angle of arrival and frequency of the interference signal is plotted in Figure 4.3. If we compare this to Figure 4.4, we see that a null of 80dB is placed exactly in the true location and frequency of the interference signal. The colormap on the right side of Figure 4.3 serves to map the plot color to the attenuation at any location. To ensure that the interference signal was fully canceled, the residual interference power left at each frequency after applying the weights was graphed. As seen in Figure 4.5, the interference signal was completely rejected.

To show the adaptive band-partitioning's insensitivity to arrival angle, a single narrow band interference signal of 15MHz was generated for arrival angles of -90° to 0°. Amazingly, the null depth remains relatively constant as the interference signal's arrival angle was varied. This can be seen in Figure 4.6. It appears that perfect cancellation is achieved even when the interference signal's arrival angle is close to the arrival angle of the desired communications signal. While this alone might be true, it is also extremely important to observe the effect of the weights on the desired signal. Figure 4.7 plots the attenuation of the desired signal for an interference signal as the arrival angle is varied as in Figure 4.6.. Surprisingly, even when the interference signal is at 0°, the desired signal is hardly attenuated. This can be accounted for by the fact that the desired signal is a spread spectrum signal having a bandwidth of 25 MHz. Thus, even though the interference signal and thus the desired signal is canceled at 15 MHz, most of the desired signal's frequency components remain intact and so too then does the desired signal.

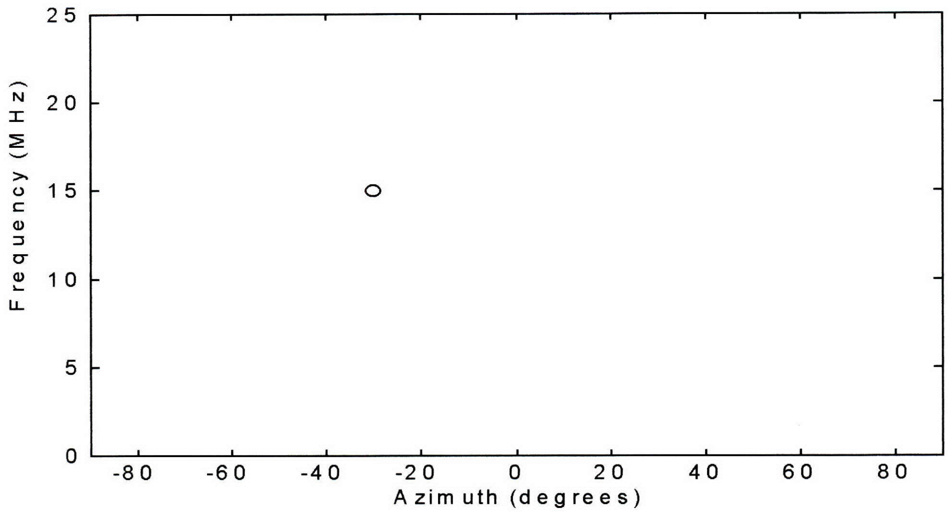

Figure 4.3 Plot of interference signal's azimuth and frequency

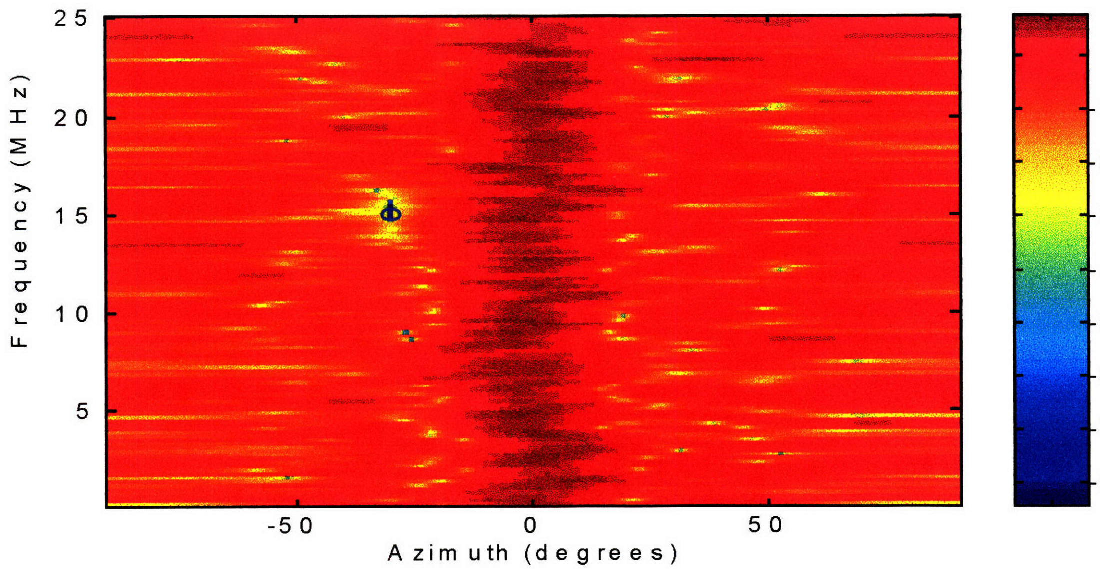

Figure 4.4 Beampattern and location for single interference signal

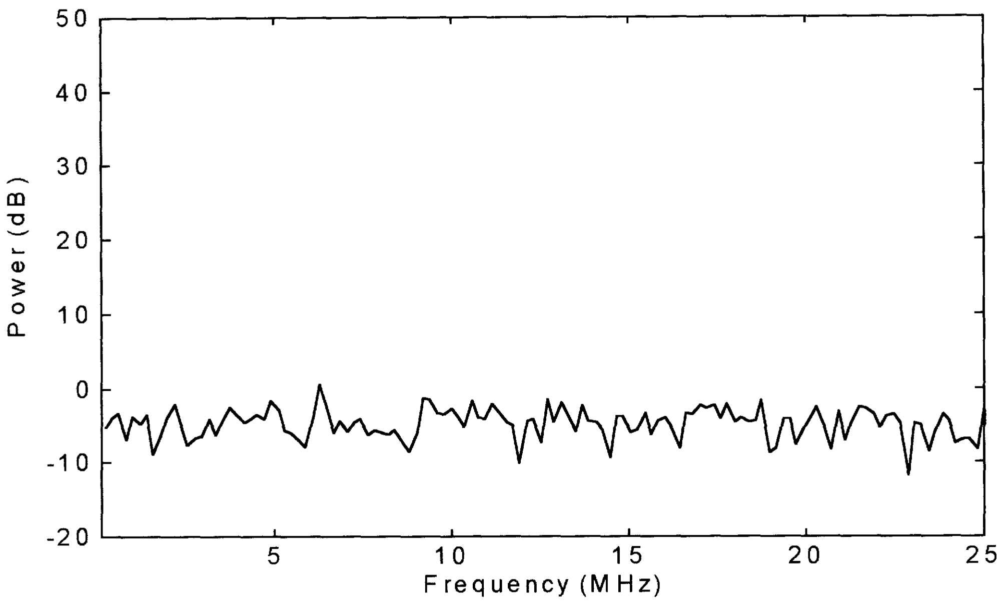

Figure 4.5 Power in frequency bins after applying weights

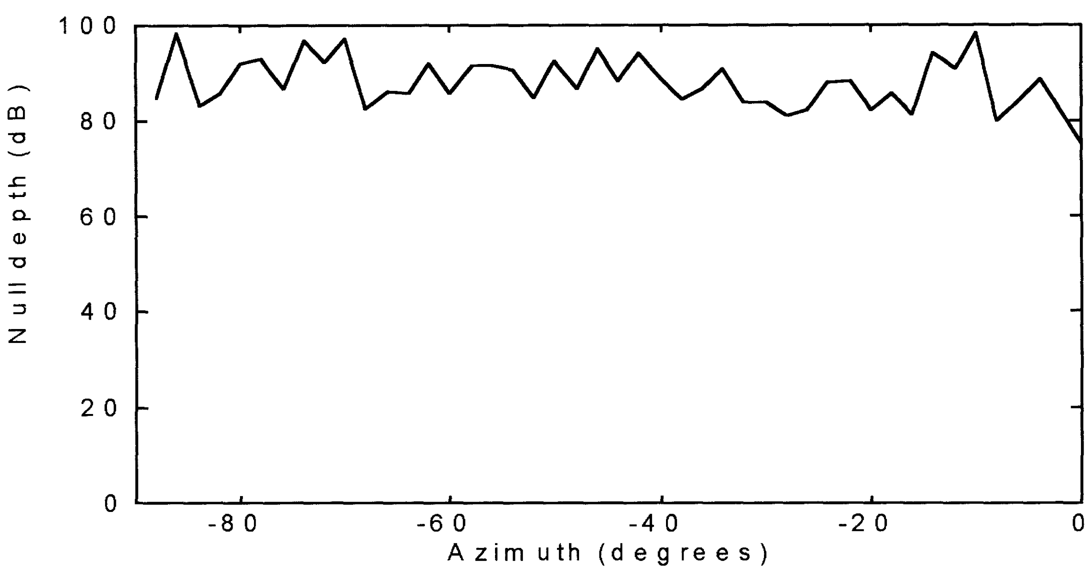

Figure 4.6 Null depth for narrowband interference signal vs. arrival angle

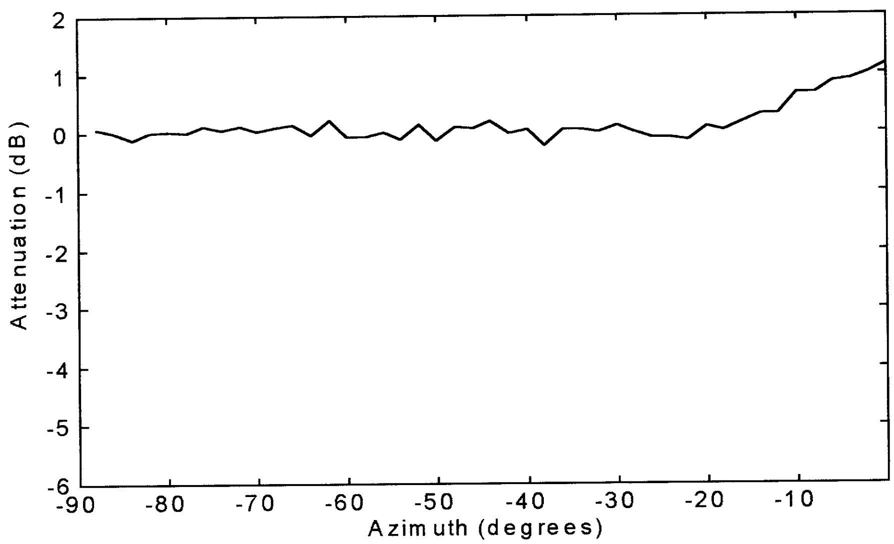

Figure 4.7 Attenuation of desired signal for single interference signal of various arrival angles

4.4.2 Multiple Narrowband Interference Signals

We have just seen that adaptive band-partitioning performs better than the classical approach when a single narrowband interference signal's arrival angle varies. The much more important advantage of band partitioning, however, becomes apparent when we have multiple narrowband interference signals. The classical approach to interference cancellation has the limit of canceling N-1 narrowband interference signals, where N is the number of array elements. In our simulations with a 5-element array, the classical approach would be able to cancel a maximum of 4 signals. In theory, the adaptive band-partitioning approach has the ability to cancel N-1 narrowband signals in each frequency bin. Implementing band-partitioning by performing 256 point FFT's, we now have 128 bins representing the frequencies of 0-25 MHz. So, our new approach should be able to cancel 4 narrowband interference signals in each of the 128 frequency bins. While this would lead us to believe that 512 narrowband signals could be canceled, this is not the entire picture. If only 4 interference signals were present in each frequency bin, then 512 signals could be canceled. Unfortunately, in practice we cannot expect a uniform distribution of interference signals across frequencies. Consequently, there is no set number of signals that the band-partitioning approach can reject. At a minimum it can cancel 4 signals. Of course, it has the ability to cancel many more. If each of the narrowband interference signals happened to fall in separate frequency bins, we would be able to cancel 512 narrowband interference signals.

To illustrate that adaptive band-partitioning can in fact cancel more interference signals than the classical approach, two sets of plots follow. The first set of plots will show the cancellation of 4 narrowband interference signals, all centered at the same frequency of 15 MHz and 60dB, but with random arrival angles. Then, the second set of plots will show the effective cancellation of 25 narrowband interference signals with randomly distributed arrival angles and center frequencies. Again, all the signals have a power of 60dB. In both scenarios, one can see that adaptive band-partitioning does an excellent job of rejecting the unwanted interference signals.

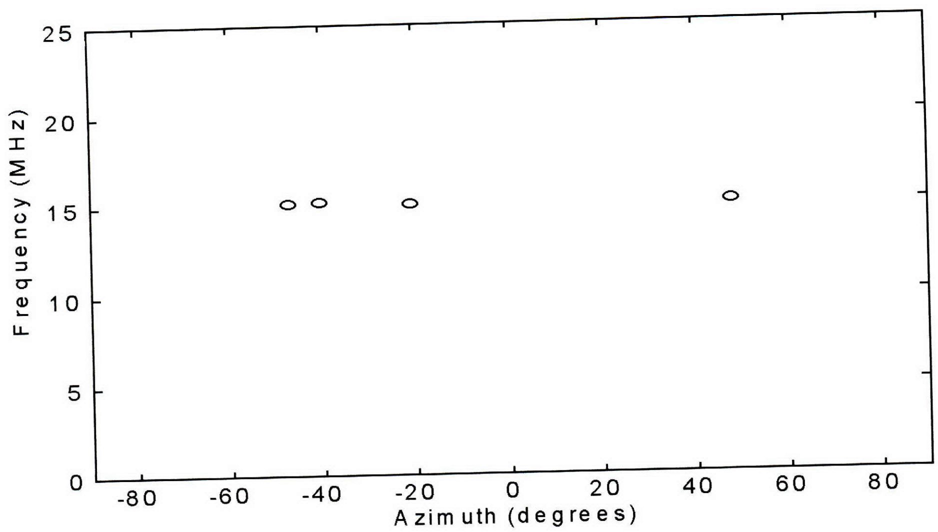

Figure 4.8 Plot of azimuth and frequency for 4 narrowband Interference signals

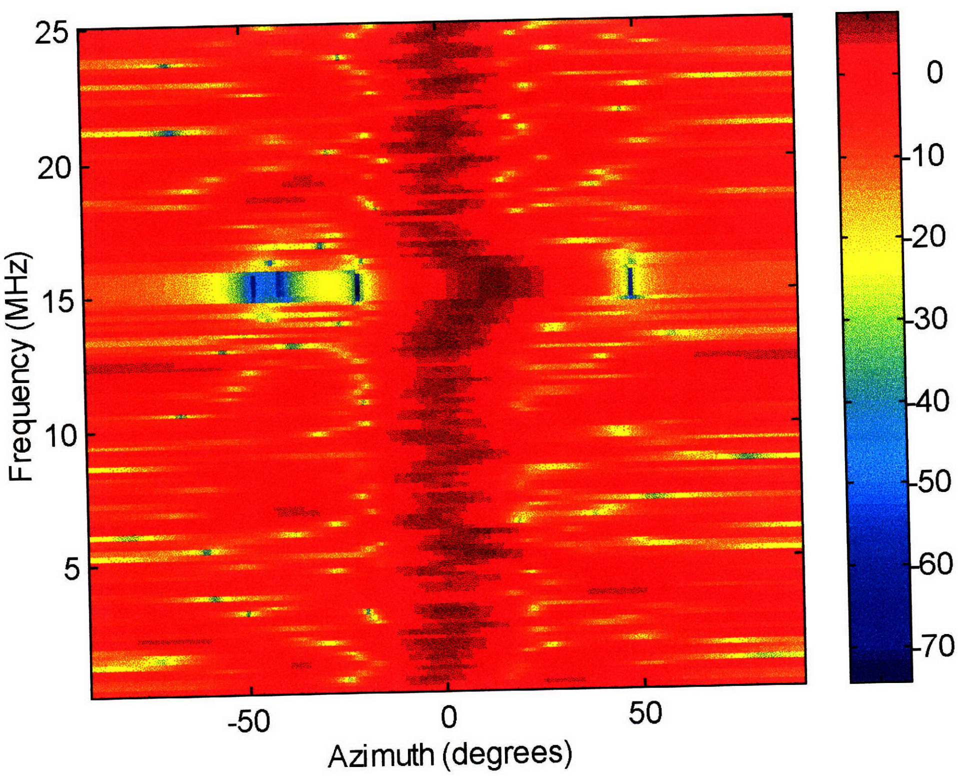

Figure 4.9 Beampattern for 4 narrowband interference signals

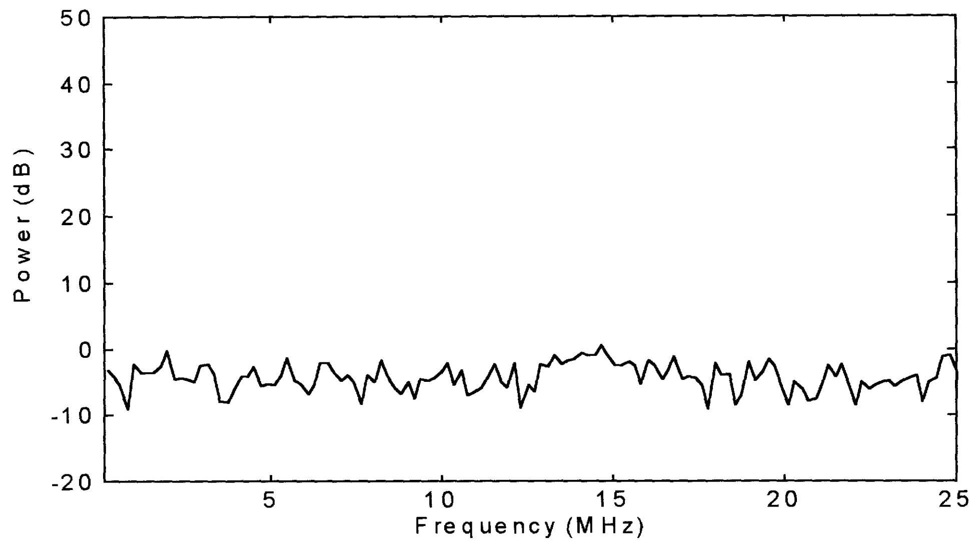

Figure 4.10 Power in frequency bins after applying weights to 4 narrowband interference signals

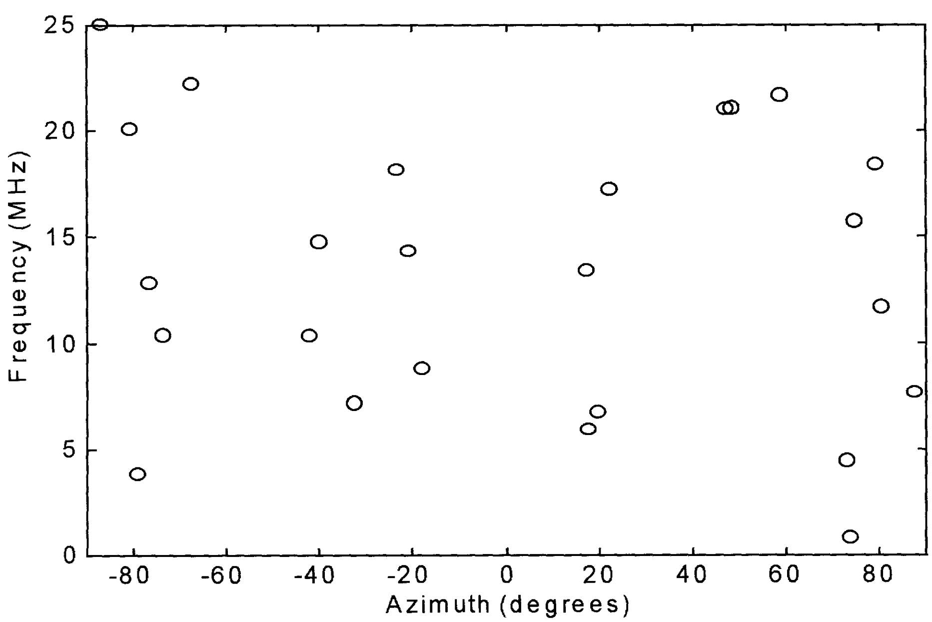

Figure 4.11 Plot of azimuth and frequency for 25 narrowband interference signals

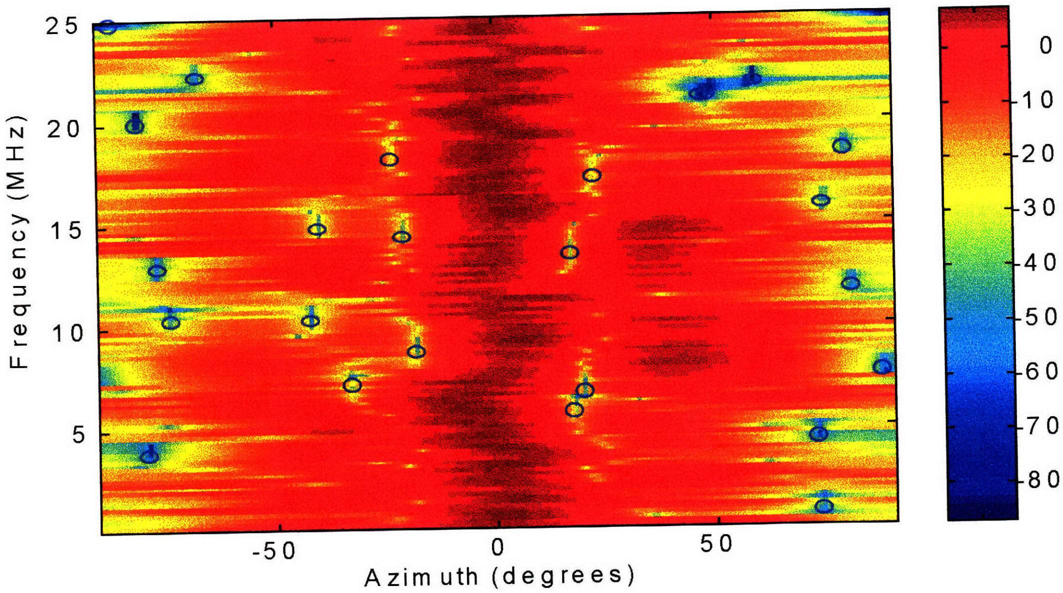

Figure 4.5 Beampattern for 25 narrowband interference signals

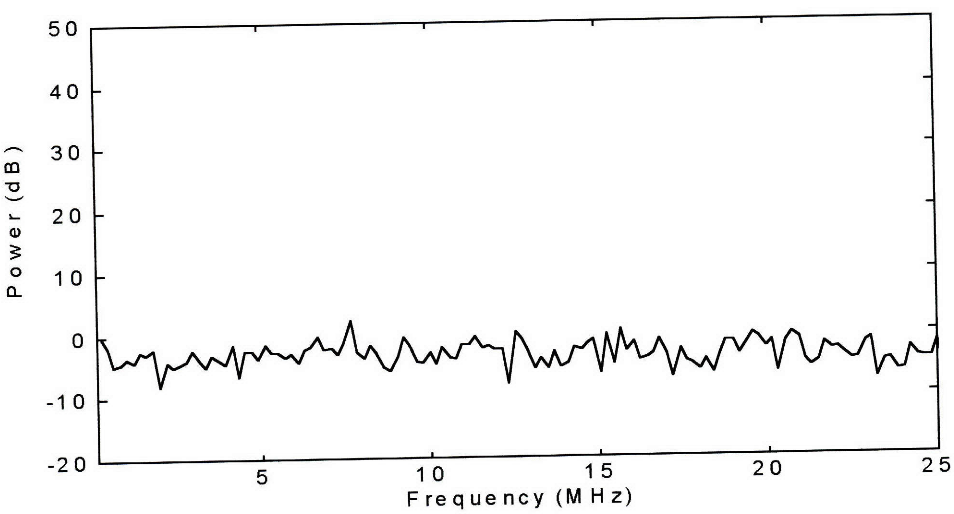

Figure 4.13 Residual power in frequency bins for 25 narrowband interferences signals after applying weights

4.4.3 Wideband Interference Signals

As illustrated in Section 2.3.1, the classical approach's Achilles tendon was the degradation of cancellation as the interference signal's bandwidth increased. This was the main motivating force behind the creation of adaptive band-partitioning. To see how well adaptive band-partitioning fairs with a interference signal having a wide bandwidth, a 60dB interference signal covering the full 25MHz bandwidth and having an arrival angle of -30° was generated. Figure 4.14 show the interferer's true location and frequency. The beampattern corresponding to the optimal cancellation weights is plotted in Figure 4.15. As we had hoped, a null is placed across all frequencies at an angle of -30°. Looking at the residual power after applying the weights, Figure 4.16, we see that adaptive band-partitioning is completely effective at canceling a wideband signal. No degradation results from attempting to cancel an interference signal with a bandwidth.

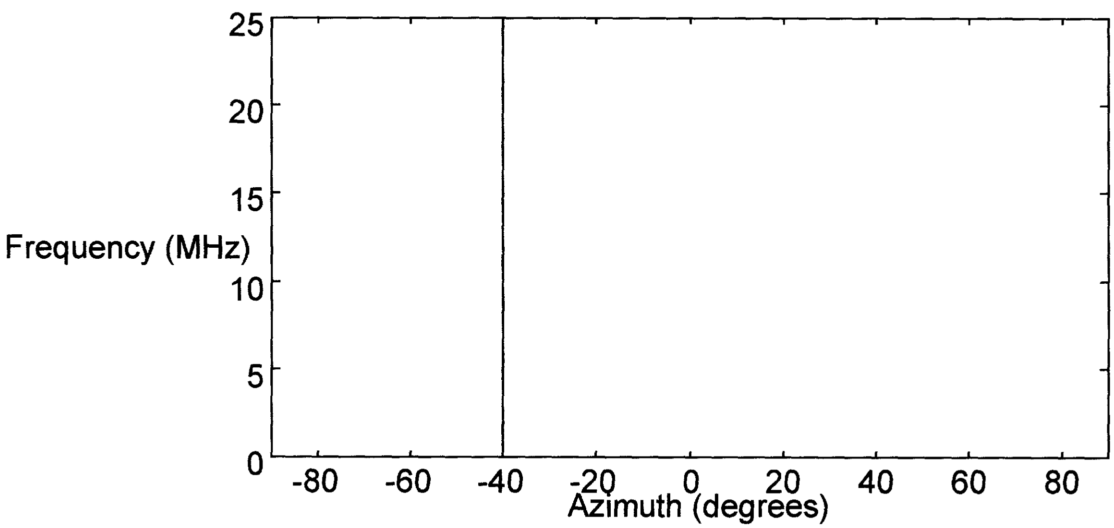

Figure 4.14 Location and frequency of single wideband interference signal

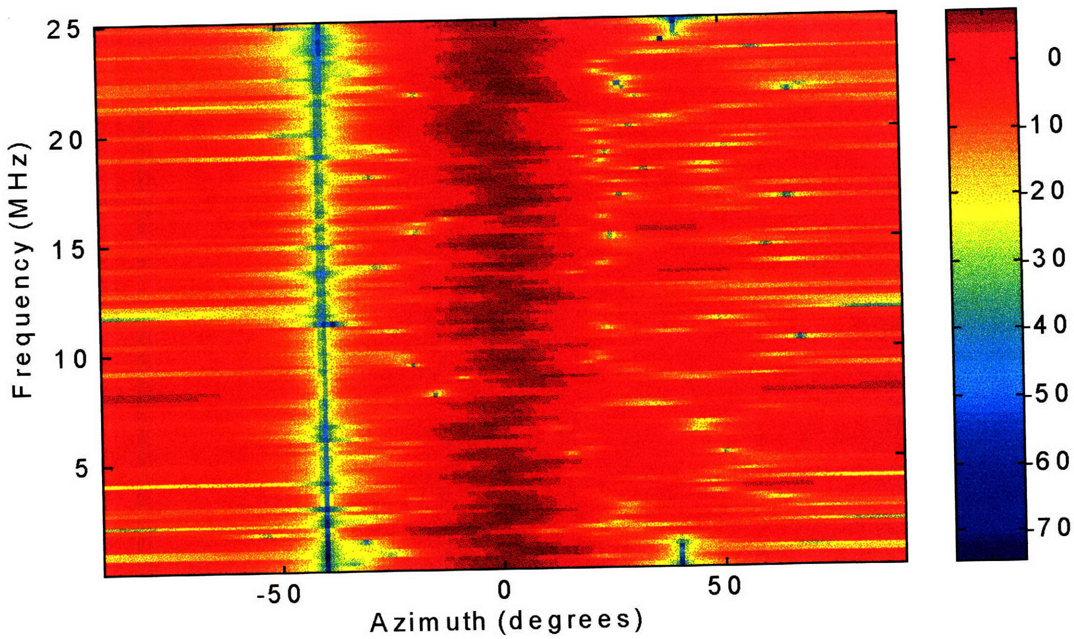

Figure 4.15 Beampattern for single wideband interference signal

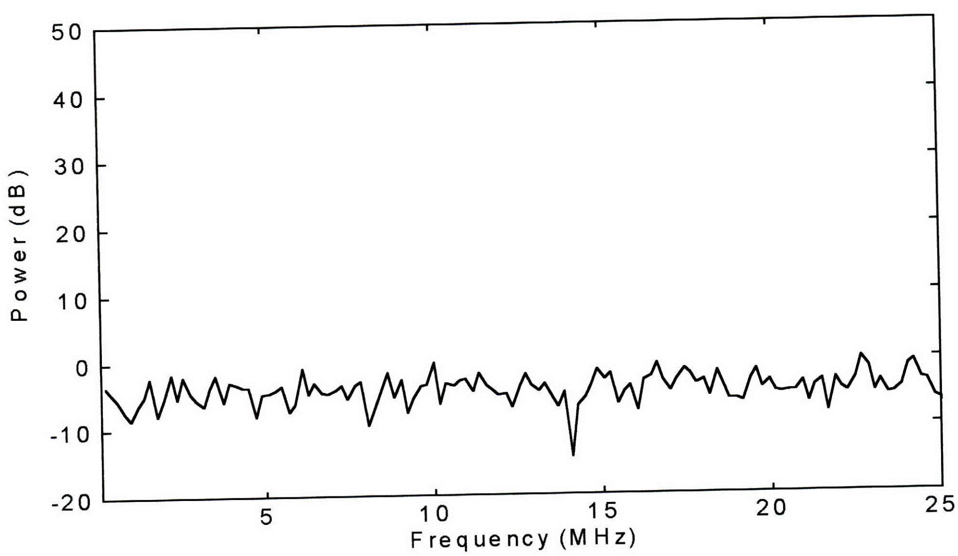

Figure 4.16 Power in each frequency bin after applying weights to single wideband interference signal

The maximum number of wideband interference signals that adaptive band-partitioning can cancel is limited to N-1. For our five element array, only four wideband signals can be canceled. While we have not gained the ability to cancel a greater number of wideband interference signals than the classical method, we are able to fully cancel a wideband interference signal, no matter how large the bandwidth. Unlike the classical method, no degradation results due to interference bandwidth. This is because optimal weights were derived for each frequency bin and each array element. The downfall of the classical approach was the use of only one complex weight per element.

To confirm the ability to cancel four wideband interference signals, adaptive band-partitioning was given four 60dB wideband signals as seen in Figures 4.17. The beampattern in Figure 4.18 shows that nulls are placed at the precise arrival angles generated. Finally, the residual power is plotted in Figure 4.19. Adaptive band-partitioning worked perfectly in canceling the four wideband signals.

To illustrate how the algorithm fails when pushed beyond the limits of its capabilities, five wideband interference signals each of 60 dB were tested. The results are shown in Figures 4.20-4.22. From the beampattern plot, it is evident that the nulls, which should be straight lines at five angles, are imperfect. The obvious indication of the failure to cancel all five interference signals is the non-zero residual power seen in Figure 4.22. Indeed, we are limited to canceling only N-1 wideband interference signals.

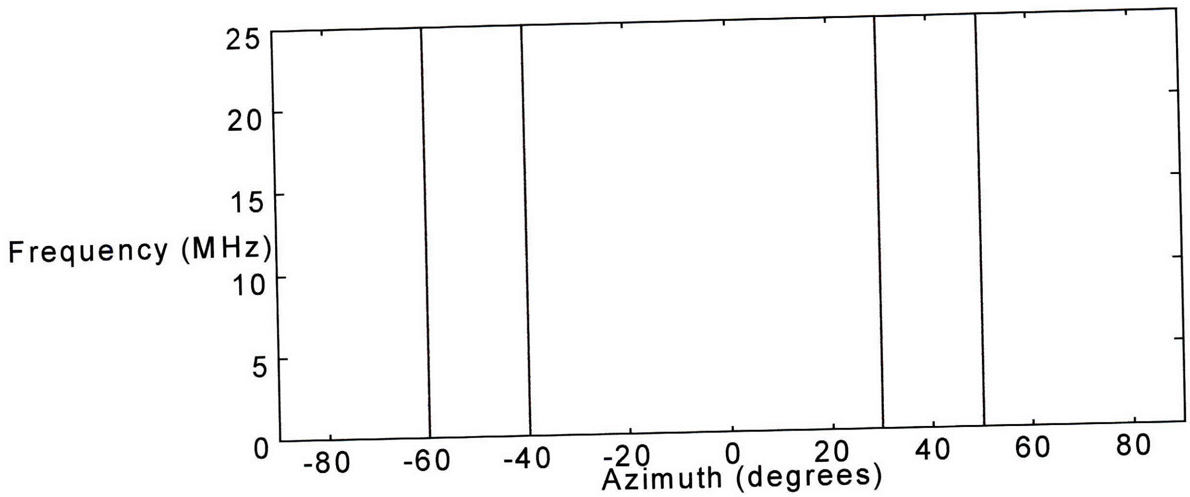

Figure 4.17 Location of four wideband interference signals

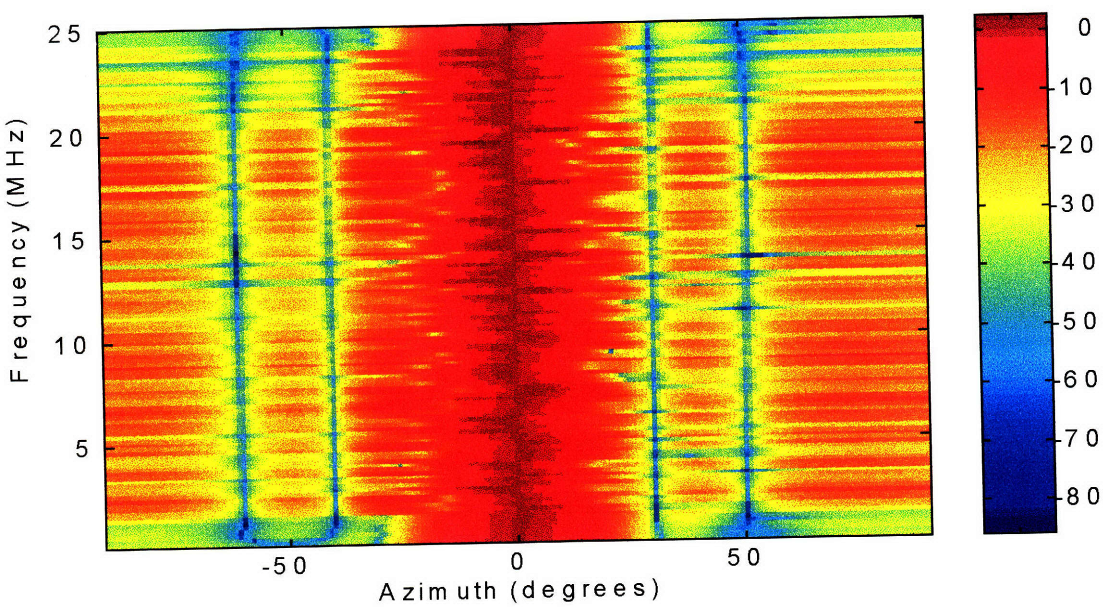

Figure 4.18 Beampattern for four wideband interference signals

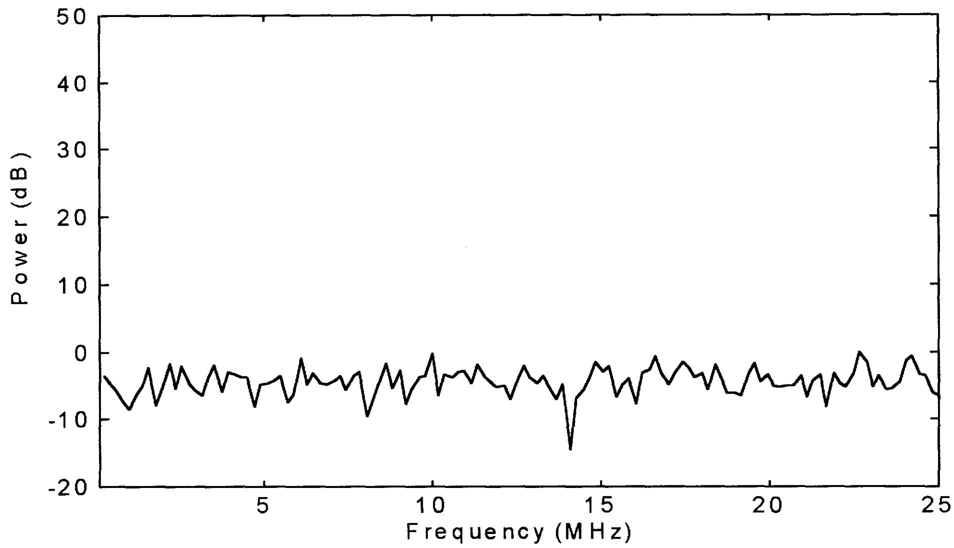

Figure 4.19 Power in each frequency bin after applying weights to four wideband interference signals

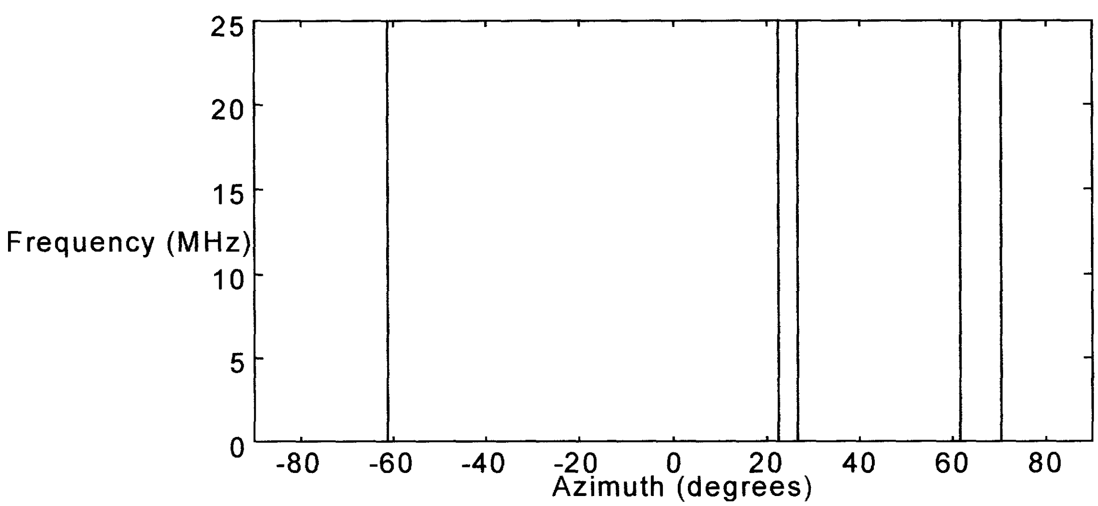

Figure 4.20 Location of 5 wideband interference signals

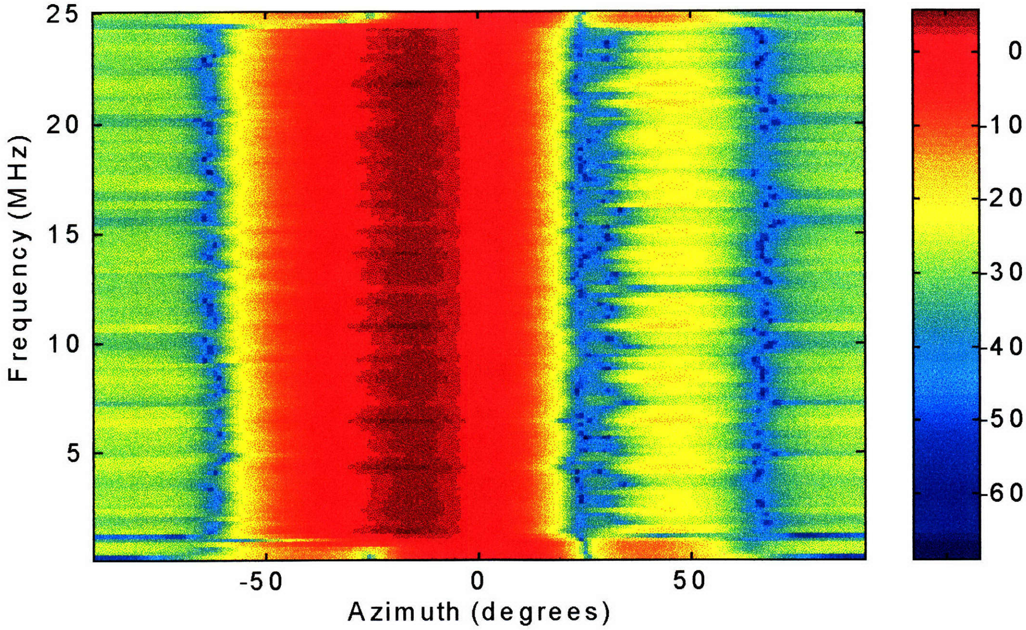

Figure 4.21 Beampattern for 5 wideband interference signals

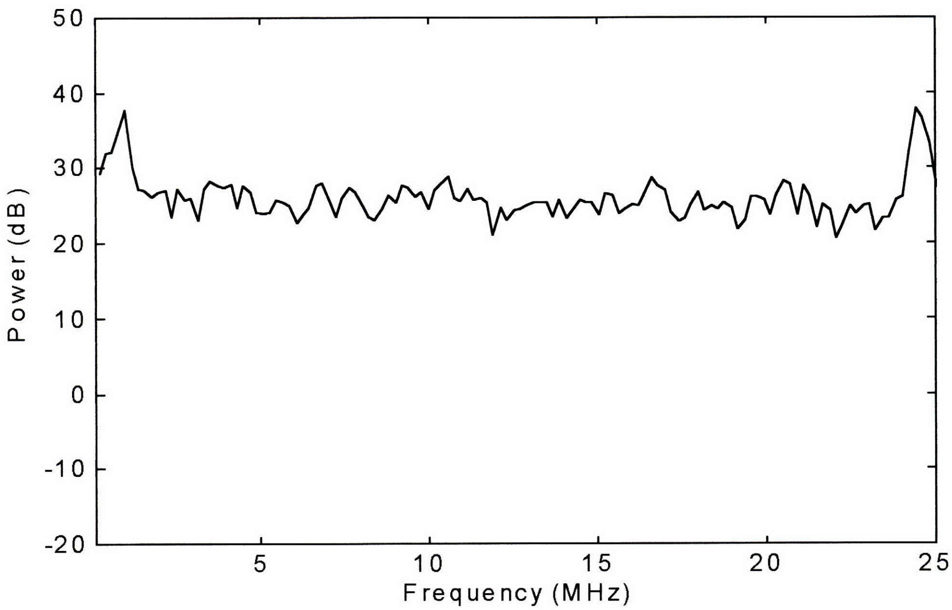

Figure 4.22 Residual interference power in each frequency bin after applying weights to 5 wideband interference signals

4.4.4 Narrowband and Wideband Interference Signals

As a final test, the adaptive band-partitioning approach was tested using both narrowband and wideband interference signals. Since we verified that at most we could cancel only four wideband interference signal, the algorithm was tested on 2 wideband and 25 narrowband interference signals, all of 60dB power. While the classical approach would have failed at five narrowband interference signals or just one wideband signal if the bandwidth was large enough, adaptive band-partitioning is capable of canceling a much larger number of interference signals. As seen in Figures 4.23-4.25, adaptive band-partitioning has no problem canceling 27 signals. As long as there are no more than four signals in each frequency bin, adaptive band-partitioning has the ability of canceling an even greater number than 27.

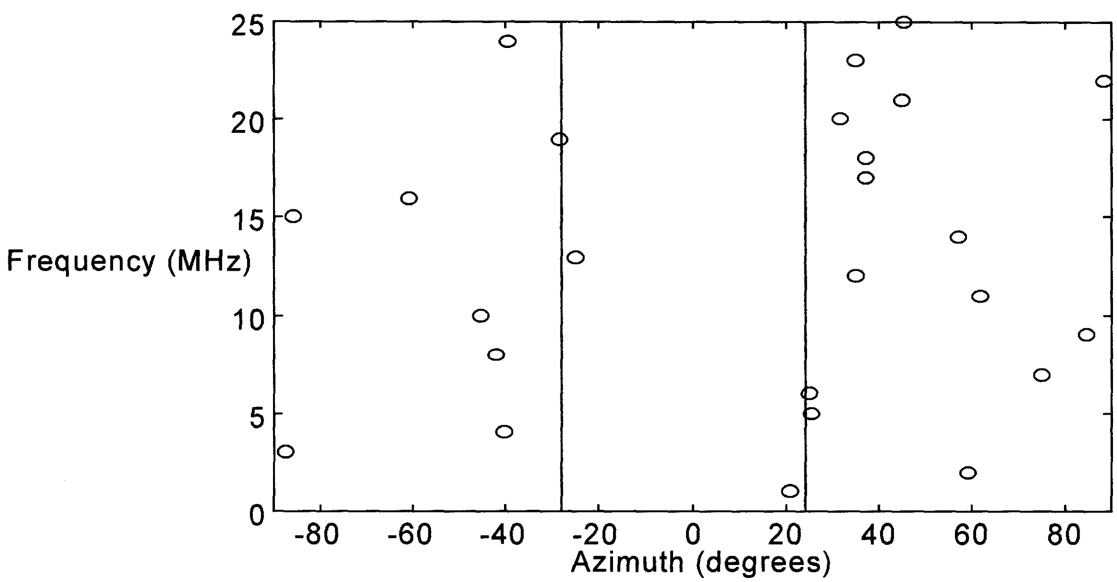

Figure 4.23 Location of 2 wideband and 25 narrowband interference signals

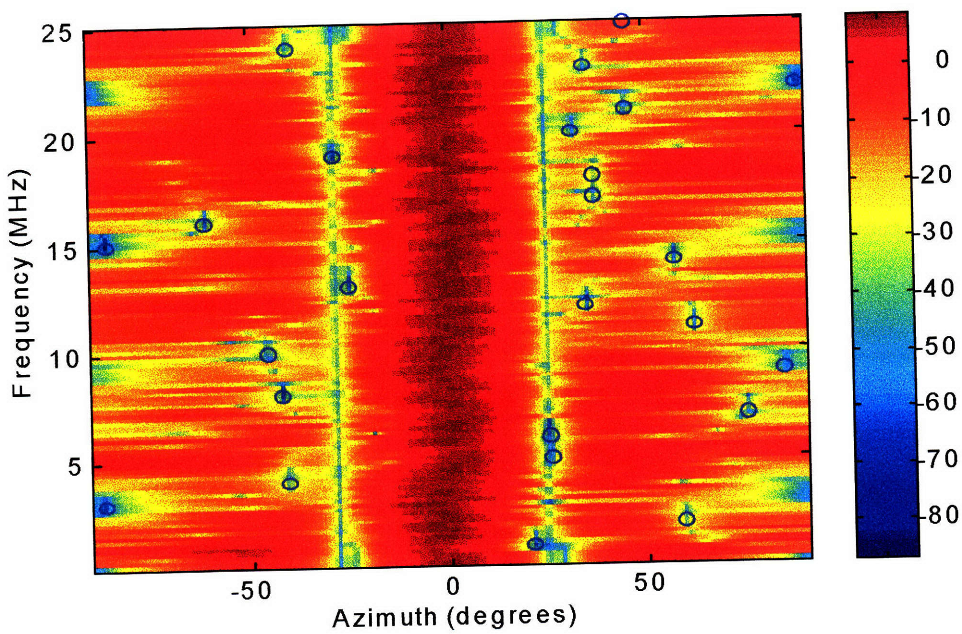

Figure 4.24 Beampattern for 2 wideband and 25 narrowband interference signals

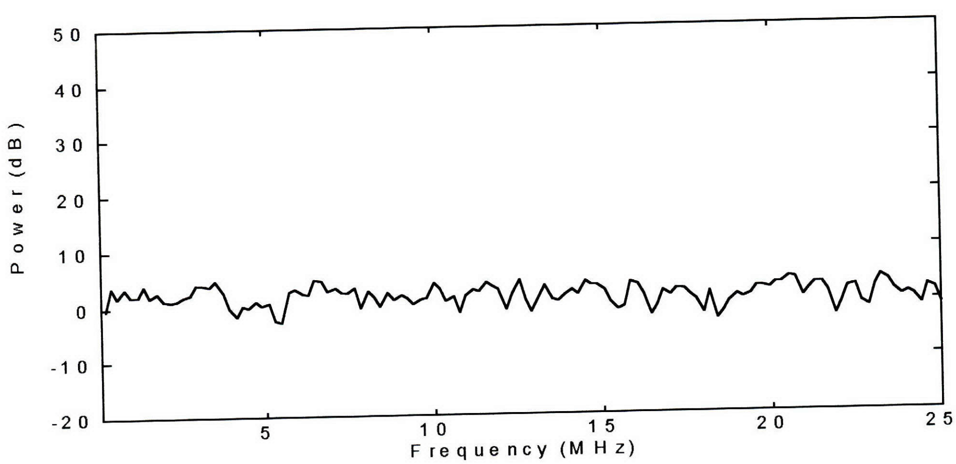

Figure 4.25 Power in each frequency bin after applying weights to 2 wideband and 25 narrowband interference signals

Chapter 5

5. Conclusion

The previous three chapters have presented the development and analysis of the standard approach to interference cancellation as well as that of adaptive band-partitioning. We began in Chapter 2 by introducing the tradeoffs inherent when choosing the array size and spacing. Then we investigated the idea of interference cancellation by creating nulls through the addition of complex weights to the elements of an array. Deriving the results of interference cancellation for a standard two-element array, we determined that applying a single complex weight to each element results in limited interference rejection. While the standard technique has the ability to completely cancel narrowband interference signals, it fails to fully cancel interference signals of appreciable bandwidth. The inability to cancel wideband interference signals instigated the investigation of a different cancellation approach, adaptive band-partitioning. Chapter 3 and Chapter 4 served to introduce the methods and algorithms necessary for the implementation of adaptive interference cancellation through the use of frequency-dependent complex weights.

5.1 Algorithm Summary

For a linear array and a stationary signal environment, we determined in Section 3.1 that the optimal steady-state weight solution found using the MSE and ML criterion had the form $\mathbf{W}_{opt} \propto \mathbf{R}_{xx}{}^{-1}\mathbf{v}^*$. Knowing that useful applications could not be expected to be characterized by stationary signal environments, we investigated two algorithms used to converge to the steady-state weight solution. We found that direct matrix inversion, while introducing added complexity and computational burden, had a significant advantage over the well studied and relatively simple to implement least-mean-squared algorithm. Recalling the derivations in Section 3.2.2.2, the DMI algorithm required only 2N time samples to come within 3dB of the optimal steady-state weight vector. Furthermore, DMI's insensitivity to eigenvalue spread, and thus its unparalleled rapid convergence to the steady-state weight vector, make it the ideal algorithm for use in adaptive interference cancellation, especially when used in adaptive band-partitioning.

5.2 Algorithm Performance

The heart of band-partitioning, the concept of dividing the frequency spectra of a communication signal into frequency bins and applying weights to each of these bins, was illustrated in Chapter 4. As was shown in numerous simulations, the performance of adaptive band-partitioning is remarkable. Adaptive band-partitioning has capability of completely canceling wideband interference signals. In addition, it was shown to cancel at least N-1 narrowband signals, matching the ability of standard cancellation techniques. Moreover, for narrowband interference signals equally distributed across frequency bins, band partitioning has the ability of canceling (N-1)L/2 interference signals.

The advantage of adaptive band-partitioning is obvious. With the ability to cancel a much greater number of narrowband interference signals and completely cancel wideband signals, adaptive band partitioning will soon become the standard approach used in interference cancellation and rejection.

5.3 Implementability

As indicated in Section 4.3.3, an issue of primary importance when considering the implementability of adaptive band partitioning is convergence rate. In a real-world system, such as that aboard a plane, the system must be computationally as simple as possible in order to derive the weight solution with minimum latency. As derived in (4.10), performing adaptive band partitioning on a communication system with a bandwidth of 25 MHz while using DMI and dividing the frequency spectra into 256 bins, requires 30.7μsec. This required time is extremely reasonable and results in only .27 inches of movement in the aircraft in the time it takes to compute the weights. While this result in itself is remarkable, we must not overlook the enormous computational burden imposed by such a system.

In such a real system, using DMI requires estimating and inverting $\mathbf{R}_{xx}$. As stated in Section 3.2.2.2, KN(N+1)/2 complex multiplications are needed in estimating $\mathbf{R}_{xx}$ while an additional $(N^3/2+N^2)$ complex multiplications are needed to calculate its inverse and another N^2 multiplications to compute the weights. To calculate a new set of weights after receiving each new input sample for a 5-element array where K=2N=10, would require roughly $3(N^2+N^3/2) = 263$ operations. Unfortunately, since we are sampling at 50 MHz, our system must be capable of performing 263 operations every 1/50MHz or rather every 20ns. Hence, our computer must perform 13.15 billion operations per second. This might seem unreasonable since conventional computers are only now breaking the barrier of 166 million operations per second. It is possible, however, to create a system capable of such speeds by designing a system that utilizes many parallel processors. Such a system was recently developed by C. M. Rader [9] using restructurable VLSI wafers capable of more 3 billion operations per second and as small as a wallet.

5.4 Future Work

There are several directions of study that might be of interest for improving the interference cancellation achieved by adaptive band-partitioning. One direction is suggested by the ability of band-partitioning to cancel (N-1)L/2 narrowband interference signals only when they happen to be distributed equally among frequency bins. To ensure that more than the minimum number of N-1 signals can be canceled, a method that adapts and divides the bins according to the distribution of interference signals could be realized. If more than N-1 interference signals happen to fall within a certain frequency bin, this bin could be further partitioned and bins devoid of interference signals could be merged together. Thus, we would always be able cancel (N-1)L/2 narrowband interference signals, no matter what their frequency distribution provided the bandwidths of the narrowband signals were close to zero.

A second area of study worthy of investigation, a bit less involved than the above mentioned method, also involves improving the ability of adaptive band-partitioning. Again, if more than N-1 narrowband signals happen to fall within the same frequency bin, cancellation cannot be achieved. We would observe residual interference power at that frequency bin. If we were to set the weights for that bin to zero, essentially zeroing that frequency bin, the interference signal and desired signal at that frequency would be completely canceled. Unfortunately, now we have lost frequency information about our desired signal. Remember, however, that our desired communication signal is placed on a spread-spectrum code. Since this spread-spectrum code occupies all frequency bins, zeroing one or even many bins should not result in signal loss. This method of zeroing bins that contain substantial residual interference power should be tested for its potential in assisting adaptive band-partitioning in its rejection of interference signals.

Finally, as more complex and computationally intensive algorithms are being developed, there is a definite need for further development of systems capable of tremendous speeds, performing billions of operations per second.

References

1. R. T. Compton, Adaptive Antennas, Concepts and Performance. Prentice Hall, 1988.
2. Berard Windrow and Samuel D. Stearns, Adaptive Signal Processing. Prentice Hall, 1985.
3. J. E. Hudson, Adaptive Array Principles. Peter Peregrinus Ltd., 1981.
4. M. J. Levin, "Maximum-Likelihood Array Processing," Lincoln Laboratories, MIT, Lexington, MA, Semiannual Technical Summary Report on Seismic Discrimination, December 31, 1964.
5. I. S. Reed, J. D. Mallett, and L. E. Brennan, "Sample Matrix Inversion Technique," Processing of the 1974 Adaptive Antenna Systems Workshop, March 11-13, Volume I, NRL Report 7803, Naval Research Laboratory, Washington, DC, pp. 219-222.
6. I. S. Reed, J. D. Mallet, and L. E. Brennan, "Rapid Convergence Rate in Adaptive Arrays," *IEEE Trans. Aerosp. Electron. Syst.*, Vol. AES-10, No. 6, pp. 853-863, November 1974.
7. Don. H. Johnson and Dan E. Dudgeon, Array Signal Processing, Concepts and Techniques. Prentice Hall, 1993.
8. Alan V. Oppenheim and Ronald W. Schafer, Discrete-Time Signal Processing. Prentice Hall, 1989.
9. C. M. Rader, "VLSI Systolic Arrays for Adaptive Nulling," *IEEE Signal Processing*, pp. 29-49, July 1996.
10. R. A. Iltis and L. B. Milstein, "Approximate Statistical analysis of the Widrow LMS algorithm with application to narrow-band interference rejection," *IEEE Trans. Commun.*, Vol. COM-33, pp.121-130, Feb. 1985.